Basin Research

WILEY

Basin Research IAS EAGE

RESEARCH ARTICLE

Crustal Melting Events During the Late Stage of Syn-Rift at the Magma-Intermediate Continental Margin: A Numerical Study From the Northern South China Sea Margin

Fucheng Li[1,2,3] | Zhen Sun[1,2,3] | Hongfeng Yang[4] | Yunying Zhang[2] | Ziying Xu[1] | Lijie Wang[1]

[1]Key Laboratory of Marine Mineral Resources, Ministry of Natural and Resources, Guangzhou Marine Geological Survey, Guangzhou, China | [2]Key Laboratory of Ocean and Marginal Sea Geology, South China Sea Institute of Oceanology, Innovation Academy of South China Sea Ecology and Environmental Engineering, Chinese Academy of Sciences, Guangzhou, China | [3]China-Pakistan Joint Research Center on Earth Sciences, CAS-HEC, Islamabad, Pakistan | [4]Earth System Science Programme, Faculty of Science, The Chinese University of Hong Kong, Hong Kong, China

Correspondence: Fucheng Li (iamlifucheng@163.com) | Zhen Sun (zhensun@scsio.ac.cn)

Received: 3 September 2024 | **Revised:** 31 March 2025 | **Accepted:** 25 April 2025

Funding: This research was supported by the the Key Laboratory of Marine Mineral Resources, Ministry of Natural and Resources, Guangzhou (KLMMR-2022-G04); Ministry of Science and Technology of China (2023YFF0803402), NSFC Major Research Plan on West-Pacific Earth System Multispheric Interactions (92158205), the Hainan Provincial Natural Science Foundation of China (422MS161); the Guangdong Natural Science Foundation (2022A1515011921, 2023A151500124).

Keywords: crustal melting | magma-intermediate | numerical modelling | passive margin | South China Sea | syn-rift

ABSTRACT

The traditional distinction of magma-poor and magma-rich margins is challenged by the presence of significant late-stage rift-related magmatism in certain margins, such as the South China Sea (SCS). We use numerical modelling to investigate the conditions and processes that lead to crustal melting and the formation of high-velocity lower crustal layers (HVLs) in such magma-intermediate margins. The models demonstrate that the preferential removal of the lithospheric mantle during rifting is crucial for crustal melting, as it allows the crust to receive sufficient heat from the upwelling asthenosphere. The extent and distribution of crustal melts are influenced by extension velocity and crustal rheology, and the models reveal a strong correlation between the presence of crustal melts and thin-crust domains (< 20 km thick). The study reveals a younger-oceanward trend in magmatism, attributed to the progressive exposure of the crust to the hot asthenosphere during rifting. Comparison of modelling results with seismic observations from the SCS margin suggests that both asthenospheric and crustal melts contribute to the formation of HVLs, with crustal melts estimated to constitute approximately 15%–30%. The results not only deepen our understanding of magmatic processes in magma-intermediate margins, but also provide quantitative evidence for the classification and interpretation of passive margins.

1 | Introduction

Rifted continental margins are broadly classified as magma-rich or magma-poor based on the extent of syn-rift magmatism (e.g., White and McKenzie 1989; Planke et al. 2000; Geoffroy 2005; Pérez-Gussinyé et al. 2006, 2023; Reston 2009; Franke 2013). Magma-rich margins, often linked to large igneous provinces or hotspots, exhibit extensive volcanism, thick HVLs, and seaward-dipping reflectors (SDRs) (Coffin and Eldholm 1994). Conversely, magma-poor margins, exemplified by the Iberia-Newfoundland (e.g., Whitmarsh et al. 2001; Péron-Pinvidic and Manatschal 2009; Pérez-Gussinyé 2013; Brune et al. 2017), Brazilian (e.g., Aslanian et al. 2009; Contreras et al. 2010), and Southern Australian margins (e.g., Bronner et al. 2011; Espurt et al. 2012), display rare syn-rift magmatic additions. However, some margins blur

Summary

- In magma-intermediate margins, the preferential removal of the lithospheric mantle during late-stage syn-rift plays a crucial role in enabling crustal melting by allowing the crust to be heated by the upwelling asthenosphere.
- The study reveals a younger-oceanward trend in magmatism and a strong correlation between the presence of crustal melts and thin-crust domains (< 20 km thick).
- Comparison of modelling results with seismic observations from the SCS margin suggests that both asthenospheric and crustal melts contribute to the formation of HVLs, with crustal melts estimated to constitute approximately 15%–30%.

these categorical distinctions. The SCS margin, traditionally considered magma-poor, exhibits significant late-stage syn-rift magmatism, challenging traditional classifications (Brune et al. 2017; Larsen et al. 2018; Sun et al. 2019; Pérez-Gussinyé et al. 2023).

The prevailing classification of the SCS margin has evolved significantly, transitioning from a traditional magma-poor to a more refined interpretation that recognises its intermediate character (Sun et al. 2019; Ding et al. 2020; Pérez-Gussinyé et al. 2023). Earlier interpretations emphasised the apparent abundance of post-rift intrusions (e.g., Zhao et al. 2014; Ma et al. 2016; Fan et al. 2019; Song et al. 2017; Wang et al. 2018; Zhao, He, et al. 2018; Deng et al. 2019; Gao et al. 2019; Zeng et al. 2019; Sun et al. 2020), the absence of syn-rift magmatic products (e.g., Barckhausen and Roeser 2004; Li 2011; Franke 2013; Savva et al. 2014; Zhang et al. 2016), the extensive distribution of highly extended crust, and the presence of deep mantle-penetrating detachment faults (Dong et al. 2014; Zhao, Ren, et al. 2018; Lei, Alves, et al. 2019, Lei et al. 2020; Deng et al. 2020; Fang et al. 2022; Ye et al. 2022), which collectively led to its classification as magma-poor. However, recent advances in seismic imaging and deep-sea drilling expeditions have provided compelling evidence for substantial, though localised and rapid, late-stage syn-rift magmatism in the SCS margin (Larsen et al. 2018; Sun et al. 2019; Ding et al. 2020; Zhang et al. 2021, 2023; Pérez-Gussinyé et al. 2023). The observed syn-rift magmatism is predominantly focused beneath the continent-ocean transition zone (COT) (Geoffroy 2005; Lei, Ren, et al. 2019; Sun et al. 2019; Tugend et al. 2020), in contrast to the more extensive magmatic activity typically found at magma-rich margins (Menzies et al. 2002). Geochemical analyses of volcanic rocks from IODP drilling sites, exhibiting compositions similar to average continental crust, indicate a significant contribution of SCS continental crust to the syn-rift magma source (Zhang et al. 2018; Chen et al. 2022). The crustal contribution is further supported by the presence of 32.0 ± 1.4 Ma dacite tuff in industrial borehole LF1-1-1 (Li and Liang 1994), indicative of crustal melting above a heat source during the Oligocene (Streckeisen 1979). Consequently, the SCS also differs from typical magma-rich margins in its thinner syn-rift magmatic products, which are likely derived from both asthenospheric and crustal melting, the lack of SDRs, and the more localised distribution of magmatism.

In summary, the late-stage syn-rift magmatism in the SCS is characterised by (1) its restriction to the thin-crust domain, (2) short-lived events, (3) a dual origin from both asthenospheric and crustal sources, and (4) being highly concentrated in the eastern region. These distinctive magmatic features support an intermediate classification for the SCS margin, distinguishing it from the classic magma-rich or magma-poor categories. However, the current understanding of these characteristics is primarily based on seismic interpretations, and a quantitative framework for evaluating the driving and evolutionary processes of the intermediate margin type remains to be developed.

Over the past decade, numerous numerical models of continental extension have been developed to investigate the evolution of rifting (e.g., Huismans and Beaumont 2003; Bialas and Buck 2009; Crameri and Kaus 2010; Brune et al. 2016; Le Pourhiet et al. 2018; Tetreault and Buiter 2018; Duclaux et al. 2020; Liu et al. 2022). Most of these studies have focused on understanding how variations in physical parameters influence the development of structures and sedimentary architecture, while some have investigated the interactions between magmatic and structural processes in magma-rich environments (Lundin et al. 2018; Koptev et al. 2021; Lu and Huismans 2022). The generation of melting in magma-poor environments has been comparatively understudied, despite its significance in understanding magmatic processes. However, recent research has addressed this topic. For instance, Ros et al. (2017) explored the role of the lower crust in regulating mantle-derived magmatic products during rifting.

The partial melting of crustal rocks is commonly attributed to crustal thickening or delamination of the lower crust in orogenic belts at depths exceeding 50 km, which leads to the fertile crust reaching its solidus temperature (e.g., Ma et al. 2015; Liu, Morgan, et al. 2018; Liu et al. 2023). However, the conditions under which magma-intermediate margins incorporate crustal magmatic activity during late-stage rifting, and the contribution of such activity to HVLs, remain poorly understood. Furthermore, quantitative investigations into the distribution and age variations of crustal melts in magma-intermediate margins are lacking.

To address these unresolved questions, we employ numerical 2D forward modelling to simulate the late-stage syn-rift magmatic activities that characterise magma-intermediate margins, with a specific focus on the SCS margin. The objectives of this modelling approach are to explore the conditions that facilitate crustal magmatic activity and to investigate the influence of varying extension rates, lithospheric rheology, and geothermal conditions on the development of such magmatism. Furthermore, we will compare our modelling results with seismic profiles to estimate the relative contributions of asthenospheric and crustal melts to the formation of HVLs. Our research aims to deepen our understanding of igneous processes associated with magma-intermediate margins, offering valuable insights that could lead to a more precise classification of passive margins.

2 | Geological Backgrounds and Rift Magmatism in the SCS Margin

The SCS margin, located southeast of the Eurasian continent, is a passive margin formed through the rifting of the South

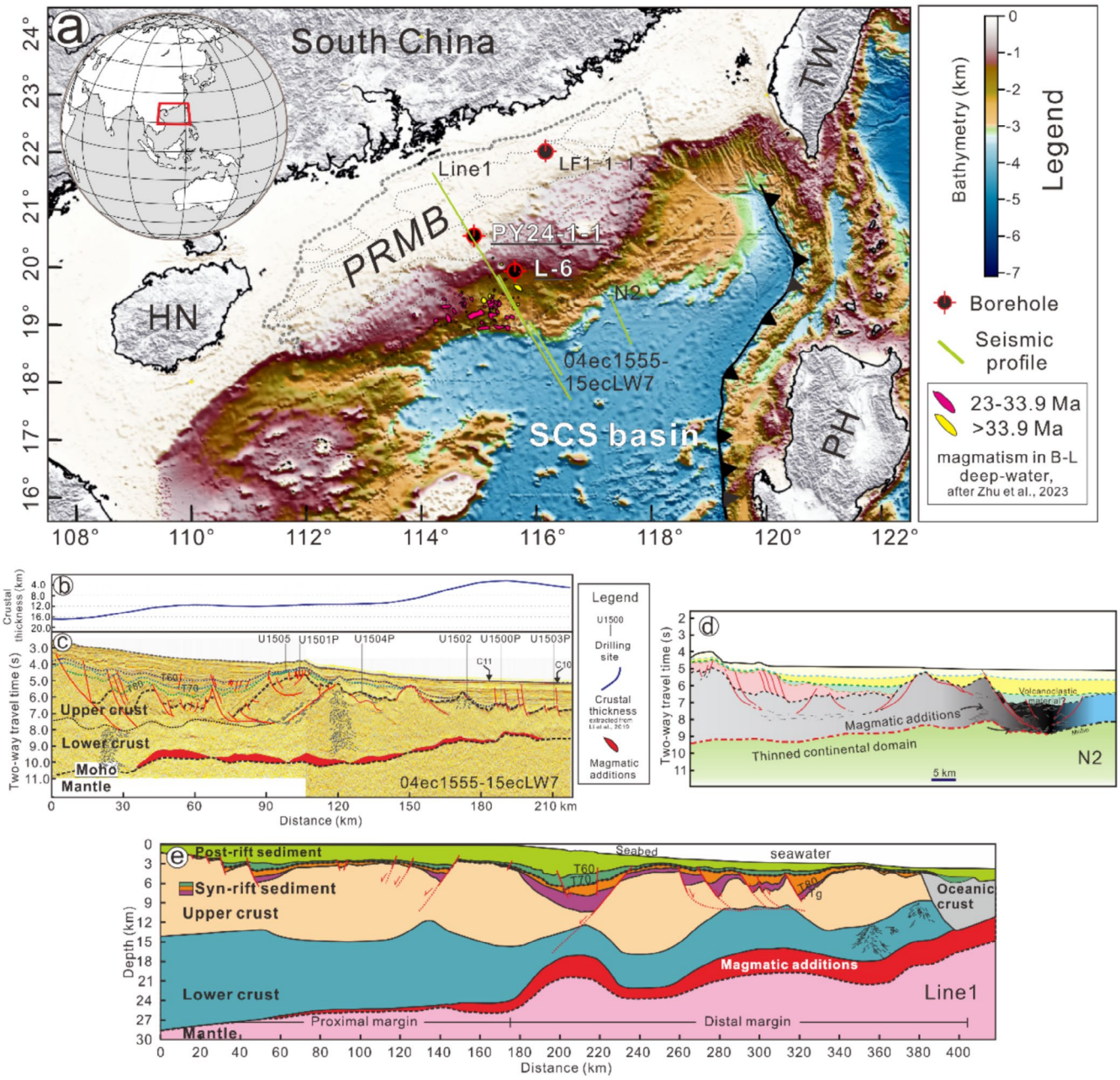

FIGURE 1 | Integrated geophysical and geological data for the northern SCS margin, including bathymetry with boreholes (a), crustal thickness (b) (extracted from Li et al. 2019), and seismic profiles 04ec1555-15ecLW7 (c) (interpreted after Sun et al. 2019), Line 1 (e) (modified after Zhao et al. 2022), and N2 (d) (modified after Ding et al. 2020) with interpreted magmatic reflectors. TW: Taiwan, PH: Philippine, HN: Hainan.

China block (Figure 1a) (Taylor and Hayes 1983; Li et al. 2018). Following the breakup of the South China block, seafloor spreading initiated in the east and northwest SCS sub-basins at approximately 33 Ma and subsequently propagated to the southwest SCS sub-basin at around 23.6 Ma (Taylor and Hayes 1983; Li et al. 2014). The SCS margin exhibits multiple phases of magmatic activity, dominated by late Mesozoic arc magmatism (e.g., Zhou and Yao 2009; Li et al. 2018) and post-rift intrusions (e.g., Zhao et al. 2014; Ma et al. 2016; Fan et al. 2019; Song et al. 2017; Wang et al. 2018; Zhao, He, et al. 2018; Deng et al. 2019; Gao et al. 2019; Zeng et al. 2019; Sun et al. 2020), with limited syn-rift magmatism. The apparent scarcity of syn-rift igneous activity previously supported its classification as a magma-poor margin (e.g., Barckhausen and Roeser 2004; Li 2011; Franke 2013; Savva et al. 2014; Zhang et al. 2016). The view of the SCS margin as magma-poor has been challenged by alternative interpretations. For instance, the presence of high-velocity lower crustal layers, detected in refraction seismic profiles, has been proposed as evidence of rift-related magmatism during the Cenozoic (e.g., Wang et al. 2006; Wei et al. 2011; Lester et al. 2014; Wan et al. 2017; Liu, Zhao, et al. 2018; Wan et al. 2019; Fan et al. 2019). These syn-rift magmatic additions in the northern SCS margin varied along the strike, as revealed by wide-angle seismic profiles. The eastern regions, including the Pearl River Mouth Basin and Tainan Basin, exhibit more significant magmatic additions compared to the western Qiongdongnan Basin (see the discussion section for the reference lists). Moreover, the availability of new, high-quality seismic data has significantly improved the identification

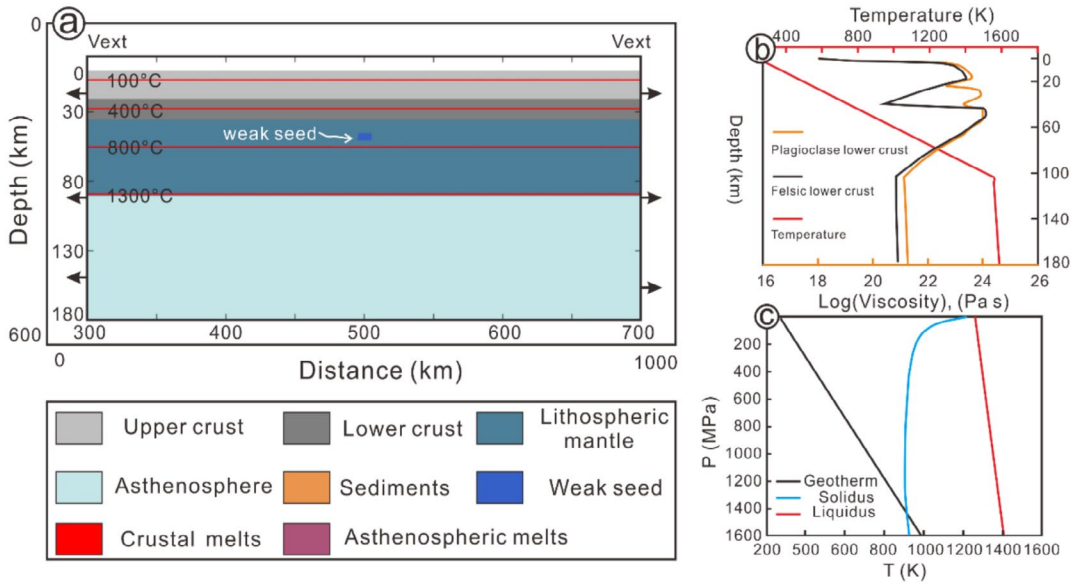

FIGURE 2 | Initial model setup. (a) An enlarged 400 km × 200 km section of the initial 1000 km × 600 km model, illustrating its composition, boundary conditions, and initial temperature distribution (red lines). (b) The yield strength profile (yellow and black line) and temperature distribution (red line) within the model. (c) The geotherm, solidus, and liquidus of the upper crust as a function of pressure and temperature.

and interpretation of magmatic reflectors within the SCS margin. These findings suggest that the SCS experienced substantial rift-related magmatism, with magmatic additions concentrated in short-duration events during the late syn-rift stage (Larsen et al. 2018; Sun et al. 2019; Ding et al. 2020; Zhang et al. 2021, 2023; Pérez-Gussinyé et al. 2023).

Three long composite seismic reflection profiles (lines 04ec1555-15ecLW7, Line 1, and N2) that cross the COT of the northern SCS margin are exhibited to characterise the diverse magmatic reflectors present (Figure 1) (Sun et al. 2019; Ding et al. 2020; Zhao et al. 2022). The seismic data reveal various discontinuous reflections with moderate to high amplitudes above the Moho, particularly in line 04ec1555-15ecLW7, which thicken landward and are interpreted as magmatic additions (Figure 1c). These reflections, potentially indicative of magmatic underplating, have been linked to melting events at the distal margin during the final phase of syn-rift (Sun et al. 2019). Similar magmatic reflectors have been identified in other seismic studies of the SCS margin (Figure 1d,e) (Ding et al. 2020; Zhang et al. 2021; Zhao et al. 2022). Furthermore, these magmatic additions within the COT have been characterised as rapid events occurring during the late stages of continental extension, likely resulting from decompression melting associated with the upwelling of hot asthenosphere (Larsen et al. 2018; Ding et al. 2020; Nirrengarten et al. 2020). These interpretations are supported by drilling results from IODP Expeditions 367 and 368, and further constrained by drilling and seismic volcano-stratigraphy in the Baiyun-Liwan deep-water area, which suggests significant magmatic activity during late-stage rifting around 33.9 Ma (Figure 1a, Zhu et al. 2023).

Seismic studies reveal that the SCS margin differs significantly from typical magma-poor margins, exhibiting substantial rift-related volcanism, particularly in the late syn-rift stages, but lacking exhumed mantle. The SCS margin also shares some magmatic characteristics with magma-rich margins, but their origins differ. Magma-rich margins often exhibit extensive magmatism linked to large igneous provinces or hotspots, with thick HVLs (P-wave velocity of 7.2–7.5 km/s) and widespread SDRs (Mutter 1993; Coffin and Eldholm 1994). In contrast, the HVLs observed in the SCS margin are likely derived from both asthenospheric and crustal melting, are thinner, and the margin itself lacks SDRs. The spatial distribution of magmatic additions in the SCS is also distinct from that in typical magma-rich margins. In the SCS, magmatism is primarily concentrated beneath the COT and extends towards the distal domain (Geoffroy 2005; Lei, Ren, et al. 2019; Sun et al. 2019; Tugend et al. 2020), whereas in magma-rich margins, magmatic processes occur across a wider area, from the thin crust to the proximal domain (Menzies et al. 2002).

3 | Numerical Model Description

We perform numerical modelling using a 2D thermomechanical code modified after Gerya (2010) and Gerya and Yuen (2007), in which finite differences and marker-in-cell methods are used to solve the momentum, continuity, and heat conservation equations, assuming an incompressible medium. Refer to the supporting documentation for additional information about the governing equations and material parameters. We design an extensional model with physical dimensions of 1000 km long and 600 km thick (Figure 2a). A 20-km thick sticky air is imposed on the upper crust to act as a free surface (Crameri et al. 2012). The velocity boundary conditions for all other boundaries are all free slip.

The earlier research on the SCS, which set restrictions on the initial model thickness, served as the foundation for the models that we developed (e.g., Li et al. 2019). The initial lithospheric thickness was set at 90 km. The material properties were defined by assigning different rock types: quartzite for the upper

continental crust and either plagioclase or felsic compositions for the lower continental crust (e.g., Liao and Gerya 2015) (Figure 2b). The plastic rheology was modelled using the Drucker-Prager yield criterion, while the viscous rheology incorporated both diffusion and dislocation creep. The strength of the lithospheric and asthenospheric mantle was determined by olivine rheology. A weak zone was introduced in the middle of the model to facilitate stress localization. The surface processes in our models were calculated by employing a simplified gross-scale erosion/sedimentation law, which assumed a constant and observably acceptable sedimentation/erosion rate of 0.2 cm/yr (Burov and Cloetingh 1997).

In this study, we concentrate on the factors influencing the architecture of rifted margins, specifically the extension rate, crustal rheology, and geothermal to evaluate the correlation between crustal stretching and magmatic processes. To explore the sensitivity of our models, we performed additional tests using extension velocities of 0.65, 0.315, and 0.25 cm/yr. The rheological weakness of the continental lithosphere in the south Chinese continent, as revealed by geophysical and geochemical studies, also plays a role in controlling the width of the thinned SCS continental crust (Li et al. 2019). To accommodate the rheological weakness, a scaling factor (f) is introduced and modified to generate a weaker rheological strength compared to the base set, with strength decreasing as the scaling factor decreases (Figure 6).

The principle of the seismic interpretation on the structure dictates that once rock undergoes melting, regardless of subsequent re-solidification, seismic profiles typically display characteristic low-frequency continuous reflections with an arcuate shape and a distinct diverging internal reflection pattern. Consequently, the magmatic phases identified in the seismic profiles include any and all products of melting that occurred during the continental rifting process. To ensure accurate comparison with seismic observations, our numerical models are designed to retain a record of all melts produced at each time step, resulting in a cumulative increase in the volume of melts as rifting progresses.

Thermal histories from seismological profiles, modelled using observed subsidence via backstripping and constrained by heat flow and crustal thickness data (He et al. 2002), were combined with previous models of the SCS evolution (e.g., Le Pourhiet et al. 2018; Li et al. 2019). Based on these studies, the initial geothermal temperature at the base of the lithospheric mantle was set to 1300°C. Additionally, we tested geothermal temperatures of 1200°C, 1300°C, and 1400°C to assess the associated uncertainties and their impact on the modelling results. The asthenosphere is characterised by an adiabatic temperature gradient of 0.5°C/km (e.g., Naliboff and Buiter 2015). The solidus and liquidus temperatures for various lithologies, including wet quartzite, are determined based on experimental observations and are incorporated into the models (e.g., Poli and Schmidt 2002). The solidus temperature of the wet quartzite was given by: $T_{\text{solidus}} = 889 + 536.6/(0.03P + 1.609) + 18.21/(0.03P + 1.609)^2$ at $P < 1200$ MPa, and $T_{\text{solidus}} = 831.3 + 0.06P$ at $P > 1200$ MPa. The liquidus temperature of the wet quartzite is expressed as: $T_{\text{liquidus}} = 1262.0 + 0.09\text{P}$ (Figure 2c) (Schmidt and Poli 1998). T represents temperature and P represents pressure. The solidus and liquidus temperatures for various lithologies at different pressures, along with other relevant material parameters, are detailed in Table S1.

4 | Results

4.1 | Reference Model

Model 1, simulated with a rapid extension rate of 0.65 cm/yr, plagioclase-rich lower crust, initially exhibits the formation of a detachment fault in the crust, accommodating deformation through simple shear. The process results in a tilted crustal block and the creation of a sediment-filled basin (Figure 3a). The lithospheric mantle, in contrast, deforms by pure shear, leading to the development of a necking zone. The final stage of the model reveals extensive crustal thinning and the generation of melts due to adiabatic decompression of the upwelling asthenosphere (Figure 3d).

The model shows that at approximately ~0.7 Myr, after 9.1 km of extension, the lower crust and lithospheric mantle rupture (Figure 3b). The rupture brings the upper crust into direct contact with the rising asthenosphere, allowing heat transfer and an increase in crustal temperature. When the temperature at the base of the crust reaches or surpasses the quartzite solidus, the crust begins to melt. The initial crustal melts form at a depth of 22 km, where the temperature exceeds the solidus temperature of 915 K (Figure 3b,f). At this point, the upper crust has been stretched to a thickness of about 16–17 km (Figure 3b). By tracing the evolution path of the early melts, it is observed that the location of these early melts also marks the furthest inland extent of crustal melting observed in the model (Figure 3d).

As the extension continues, a larger area of the crust is subjected to the high temperatures of the asthenosphere, leading to an increase in the volume of crustal melts (Figure 3g). The newly generated melts primarily migrate seaward, positioning themselves beneath the increasingly thinned crust. As a result, the age of the crustal melts decreases progressively towards the distal domain. The crustal melts reach their maximum width of 50 km when the crust finally ruptures, which corresponds to the width of the thinned crustal region with a thickness of less than 17 km (Figure 3d).

4.2 | Models With Varying Extensional Velocities

The results illustrated in Figure 4 demonstrate that varying extensional velocities lead to distinct results in the models. Generally, models with lower extension velocities exhibit a smaller region of highly thinned crust and a narrower zone of magmatic addition. For example, when the velocity is set to 0.315 cm/yr, a narrow zone of hyper-extended crust develops, with approximately 35 km exposed to the asthenosphere. Consequently, the final state of model 2 shows a melt zone with a width of 35 km, significantly narrower than the 50 km observed in the model with a higher extension velocity (Figure 4c,d). In this slower extension model, crustal melting initiates at 2.2

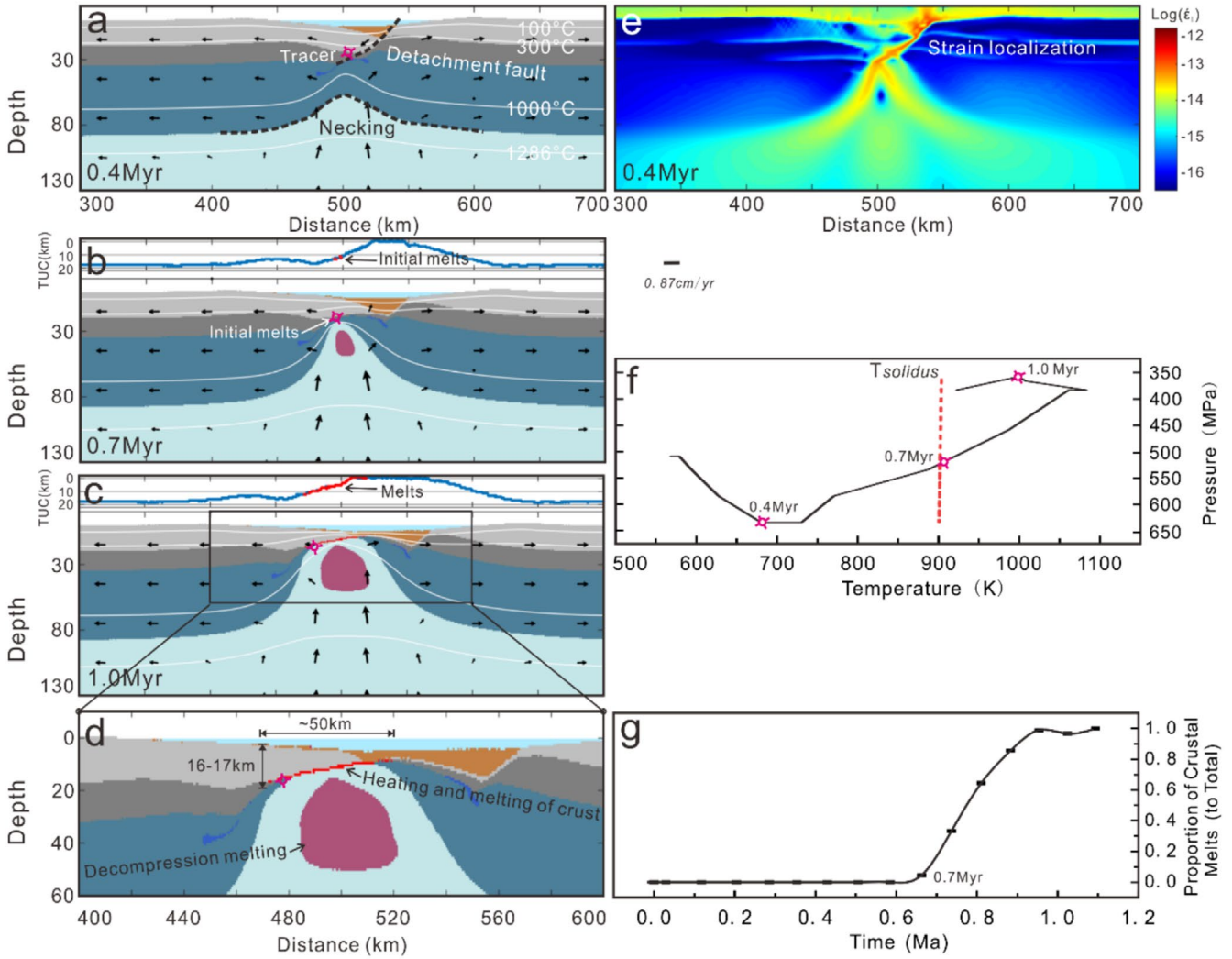

FIGURE 3 | Temporal evolution of Model 1 under rapid extension (0.65 cm/yr) and reference viscosity, showing compositional changes (a–d), strain rate at 0.4 Myr (e), P–T–t paths of representative markers (f), and the proportion of crustal melts over time (g). The abbreviation TUC refers to the thickness of the upper crust.

Myr and progressively increases towards the ocean, indicating a younger age for melts located further offshore, similar to the pattern observed in the faster extension model. At 2.8 Myr, continental rupture occurs, and the melt distribution reaches a stable configuration (Figure 4i).

When the extension velocity is further reduced to 0.25 cm/yr, the crust and lithospheric mantle rupture simultaneously, resulting in inadequate heat transfer to the crust (Figure 4e–h). The temperature of the crust, ranging from 550 to 750 K, remains below the quartzite solidus, preventing any crustal melting (Figure 4j).

Furthermore, the deformation patterns in models 2 and 3 contrast significantly during the initial extension stages. In model 2, the crust deforms through simple shear along a detachment fault, while the lithospheric mantle deforms through pure shear (Figure 5a). Conversely, model 3 experiences pure shear deformation in both the crust and lithospheric mantle, with major conjugate faults cutting through both layers (Figure 5b). It ultimately leads to the simultaneous rupture of the crust and lithospheric mantle in the final stage of model 3 (Figure 5d).

4.3 | Models With Varying Effective Viscosities

In models 5 and 6, the effective viscosity is varied to create a weaker rheological strength compared to the reference model 4 (Figure 6). The results show that both models 5 and 6 experience an extended duration of extension and a wider zone of highly thinned crust. The prolonged extension allows for a longer heating period, leading to a significant increase in crustal temperature. The elevated temperatures in models 5 and 6 result in a broader distribution of melted material beneath the extended crust. Consistent with models 1 and 2, the melts in models 5 and 6 also occur at the base of the crust, typically where it is thinner than 20 km. The widths of the crustal melts in model 5 and model 6 reach approximately 80 km and 100 km, respectively. The extended heating duration also leads to various thermal anomalies. In model 5, the edge of the thinned continental crust undergoes complete melting,

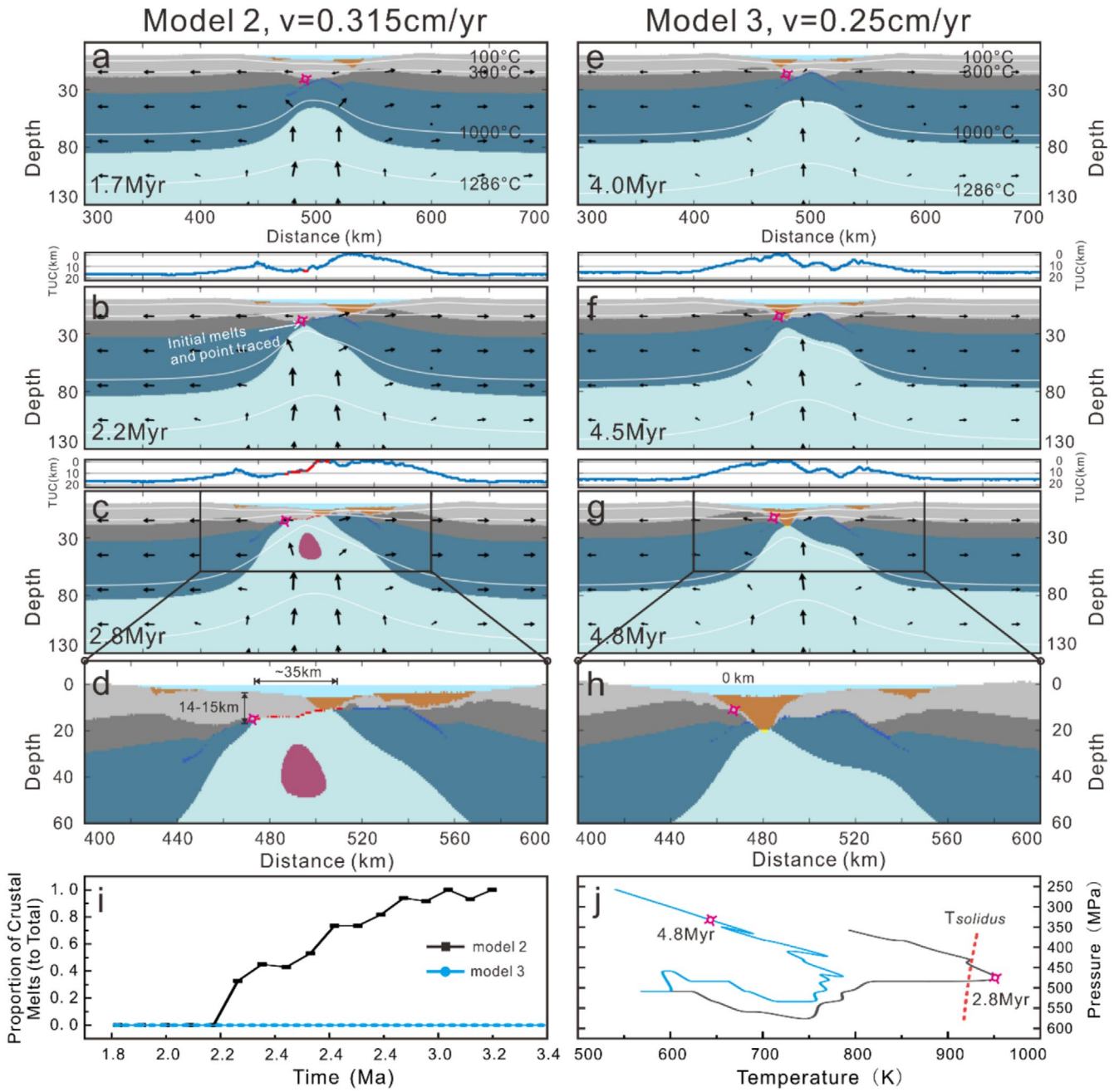

FIGURE 4 | The influence of extension velocity on rifting dynamics and melt generation, illustrated by the evolution of model 2 (a–d) at 0.315 cm/yr and model 3 (e–h) at 0.25 cm/yr. The figure includes P–T–t paths (j) and the time evolution of crustal melt proportions (i) for both models. The red dotted line in (j) represents the solidus of the representative markers, and TUC refers to the thickness of the upper crust. The abbreviation TUC refers to the thickness of the upper crust.

resulting in magmatic additions overlying it (Figure 6i). In model 6, some regions exhibit extensive melting that permeates nearly the entire crust (Figure 6l).

We further varied the extension velocities in models with different rheology. The results displayed a similar trend to the conclusions drawn in Section 4.2, where models with lower extension velocities exhibit a smaller region of highly thinned crust and a narrower zone of magmatic addition (Figure 7). In the models presented in Figure 7, which have weaker effective viscosity compared to the reference model, the lithospheric mantle in Model 10 and Model 11 ruptures before the crust, even with the lower velocity of 0.25 cm/yr. The upwelling asthenosphere heats the crust, leading to melt generation at the base of the crust (Figure 7d,h).

4.4 | Models With Varying Temperatures at the Base of the Lithospheric Mantle

With the same velocity and rheology, we varied the geothermal temperature at the base of the lithospheric mantle, testing values of 1200°C, 1300°C, and 1400°C. For models with velocities of 0.65 cm/yr and 0.315 cm/yr, higher temperatures result in a smaller region of highly thinned crust exposed to

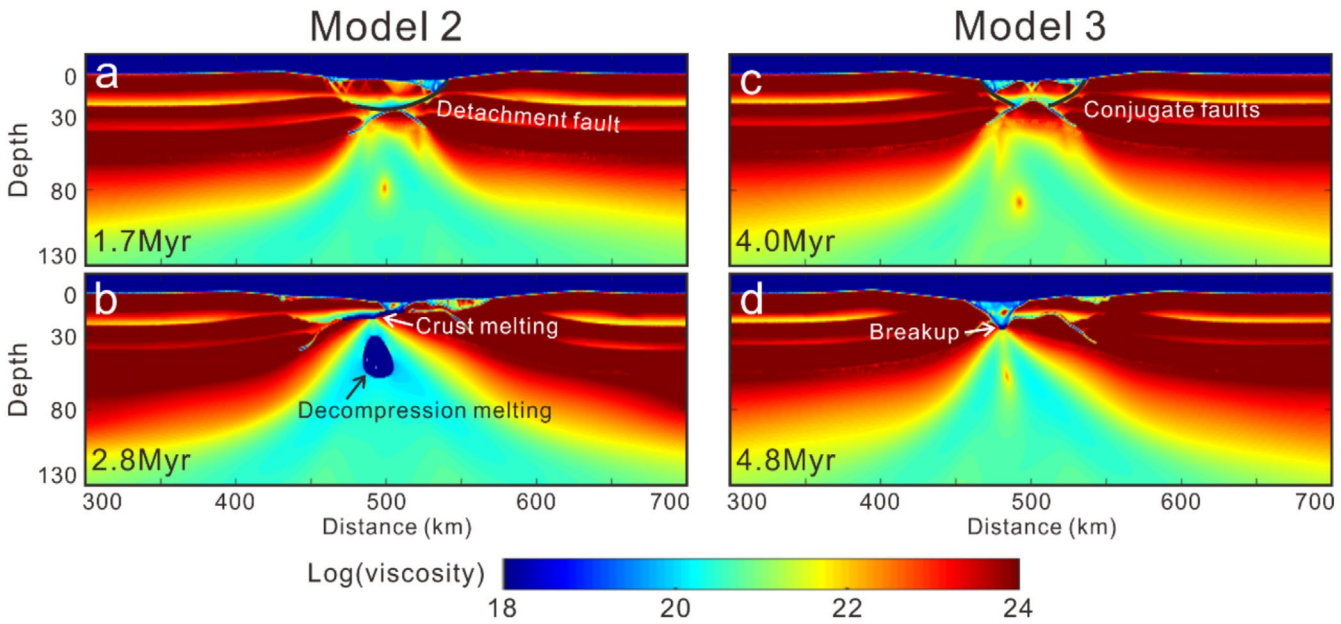

FIGURE 5 | Viscosity snapshots of contrasting deformation patterns in Model 2 (a, b) and Model 3 (c, d).

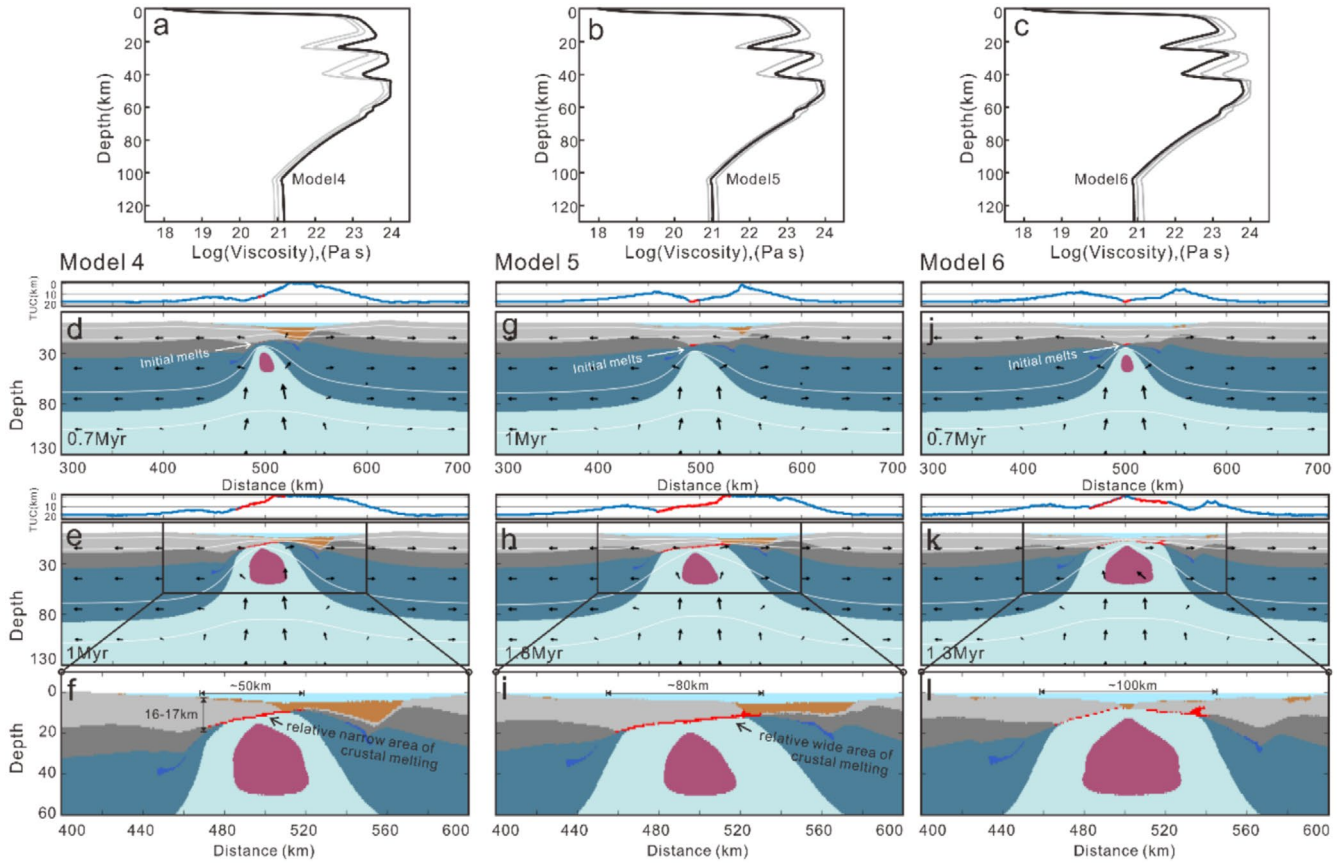

FIGURE 6 | Evolution of model 4 (d–f), model 5 (g–i), and model 6 (j–l) applied with different viscosity strengths (a–c), respectively.

the asthenosphere, leading to a narrower zone of crustal melts (Figure 8a–f). However, when the velocity decreases to 0.25 cm/yr, the models evolve similarly to Model 3, where the crust and mantle rupture simultaneously, and no crustal melting occurs, regardless of the geothermal temperature at the base of the lithospheric mantle (Figure 8g–i).

We replace the plagioclase-rich lower crust with a felsic lower crust, which exhibits weaker rheological strength (Figure 2b). Model 20 and Model 21 incorporate a felsic lower crust with basal lithospheric mantle temperatures of 1200°C and 1300°C, respectively. Consistent with the findings in Section 4.3, these models, characterised by a weaker rheology, undergo prolonged

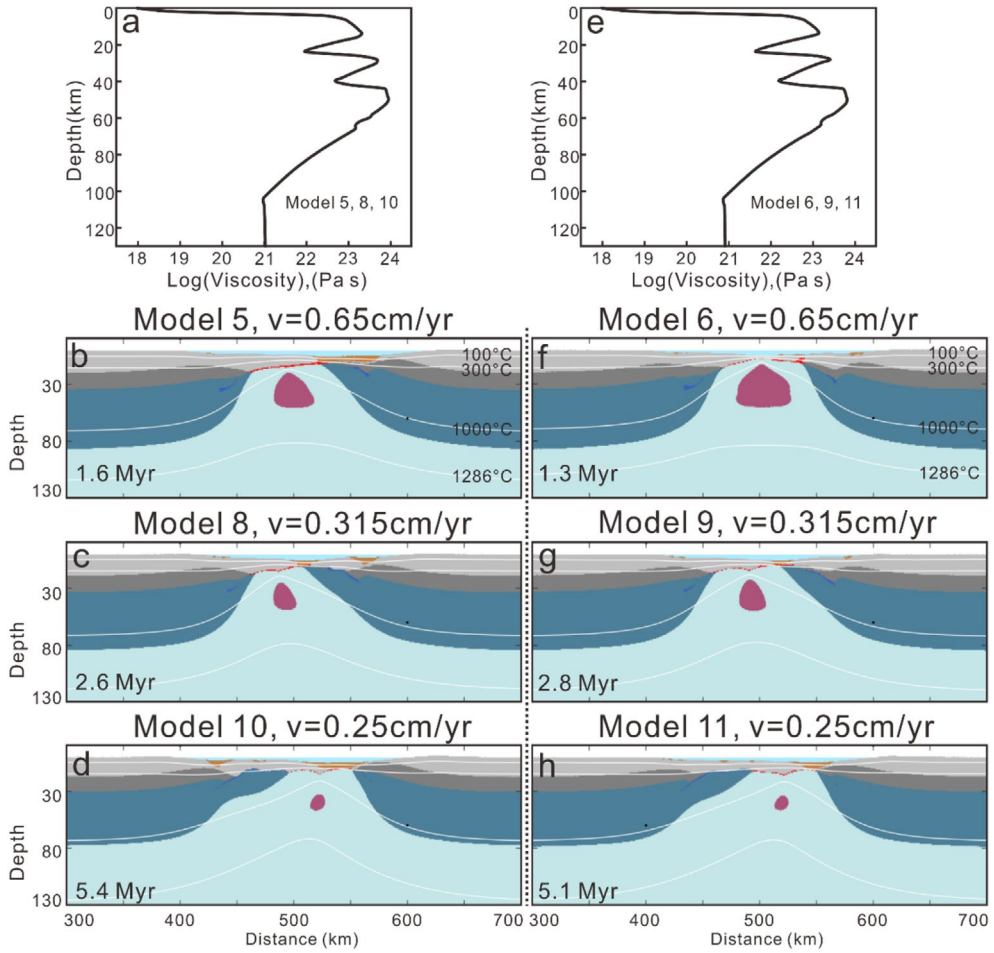

FIGURE 7 | Evolution of models with weak viscosity strength, compared to Reference Model 1, and tested with different velocities. Model 5 (b), 8 (c), 10 (d) with viscosity strength in (a), Model 6 (f), 9 (g), 11 (h) with viscosity strength in (e).

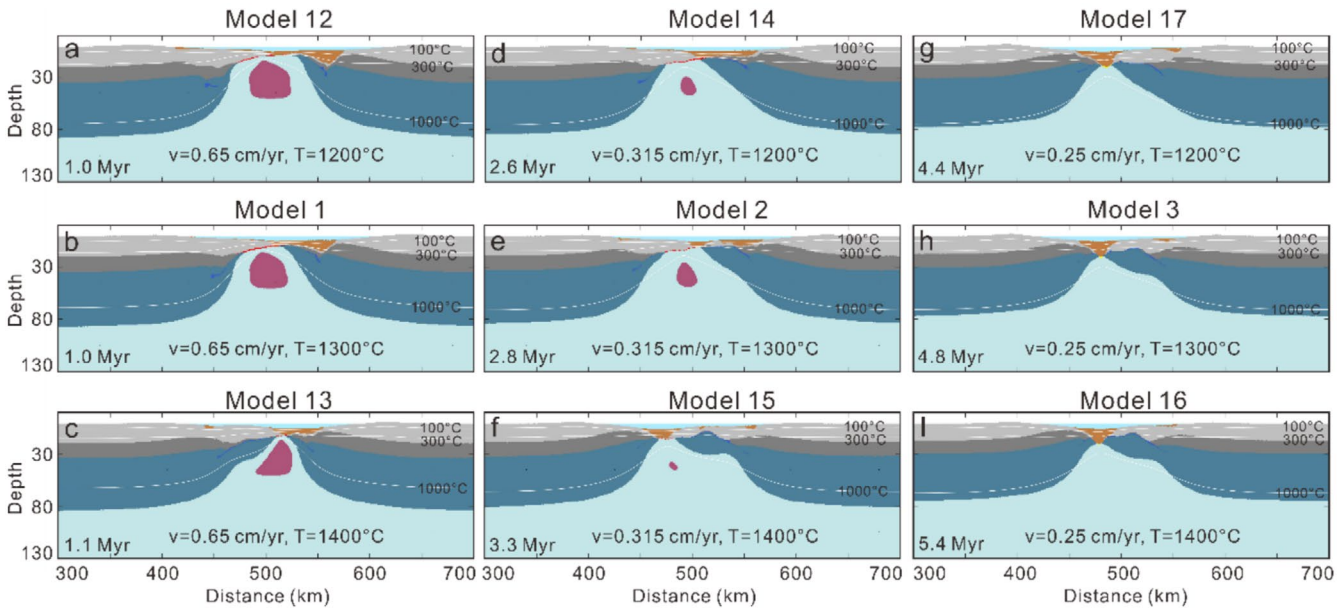

FIGURE 8 | Evolution of models with varying temperatures at the base of the lithospheric mantle. (a), (d), (g) with temperature of 1200 °C, (b), (e), (h) with temperature of 1300°C, (c), (f), (i) with temperature of 1400°C.

extension and develop a broader zone of highly thinned crust compared to cases with a plagioclase-rich lower crust. Additionally, the models exhibit a more extensive distribution of crustal melts, predominantly concentrated beneath hyper-extended domains by the end of the numerical simulations. The extension duration reaches up to 30 Myr, and the width of the

crustal melting zone extends to approximately 200 km, aligning more closely with observations from the late-stage rift evolution of the SCS margin. Notably, further modifications to the geothermal gradient appear to have minimal impact on the final crustal architecture of the rifted margins. Both Model 20, with a basal lithospheric mantle temperature of 1200°C, and Model 21, with 1300°C, display similar rift durations and comparable extents of crustal melting (Figure 9).

5 | Discussion

5.1 | Discussion on the Controlling Factors

Extension rate and lithospheric strength are key parameters that determine the final crustal architecture of rifted margins and regulate the magmatic budget during the rifting process (e.g., Huismans and Beaumont 2003; Gouiza and Paton 2019). Our research reveals similar trends and further suggests that these factors also control the spatial extent and distribution of crustal melts along the magma-intermediate margin.

The average extension rate, defined as margin width increase divided by rifting duration, is difficult to calculate precisely due to uncertainties in rift initiation timing and ages of the SCS oceanic basin (Bai et al. 2020). Our studies suggest that a rapid full extension rate, such as 13 mm/yr, can produce results consistent with observations in the SCS margin. In terms of crustal architecture, our models indicate that a high extension rate promotes strain localization, which in turn facilitates the development of low-angle detachment faults that accommodate most of the extension. Consequently, at the end of our simulations, one margin becomes markedly hyperextended while its conjugate retains much of its original crustal structure. Observations in the SCS margin support this, with seismic interpretations revealing half-graben rift basins underlain by low-angle normal faults extending downward into the Moho unconformity (Dong et al. 2014; Hayes et al. 1995; Ren et al. 2018; Zhao, Ren, et al. 2018). The SCS margin is asymmetric, with the northern margin developing a broad, hyperextended basin with significant subsidence, while the southern margin retains a thicker crust with more distributed normal faulting (Hayes and Nissen 2005). Additionally, our models show that crustal melts predominantly occur beneath the thin-crust domain, specifically where the crust is less than 20 km thick. A faster extension rate broadens the zone of highly thinned crust, which in turn promotes the production of crustal melts. These model predictions align with seismic observations from both the SCS and Namibia margins, where highly reflective seismic facies, with stratification subparallel to the Moho, have been identified beneath stretched crust, interpreted as late-stage syn-rift magmatism (Geoffroy et al. 2022; Zhao et al. 2022).

Previous numerical simulations (e.g., Brune et al. 2016) have demonstrated an initial phase of slow extension followed by a rapid increase prior to continental breakup. Plate reconstructions (e.g., Ulvrova et al. 2019) reveal similar patterns, such as the rapid pre-breakup extension of the SCS in the late Eocene. Our work focuses on magmatism during the late stage of syn-rifting, and our higher simulated rate may correspond to later rift phases characterised by increased activity. Recent seismic studies of the SCS margin indicate that magmatic additions within the COT are rapid events occurring during the late stages of continental extension (Larsen et al. 2018; Ding et al. 2020; Nirrengarten et al. 2020). Thus, our results imply that these rapid magmatic events are likely linked to the strong driving forces that promote lithospheric weakening during the rifting of the SCS margin. Despite these findings, the extension rate of the SCS is considered intermediate compared to other well-studied rift systems worldwide. For example, the Brazil–Angola margin has an extension rate of approximately 8 mm/yr (Heine et al. 2013), the Gulf of Aden rift extends at about 10 mm/yr (Brune and Autin 2013), the Red Sea Rift at 18–20 mm/yr (Viltres et al. 2020), and the Afar rift zone at roughly 20 mm/yr (Moore et al. 2021). These features position the SCS as a key transitional system in rift dynamics, demonstrating moderate extension rates, intermediate magmatic activity, and a high degree of structural complexity.

The lithospheric strength, influenced by compositional variations (e.g., felsic vs. plagioclase lower crust) and thermal structure, plays a critical role in the distribution of melted material in the SCS during rifting. A weaker lithospheric rheology promotes prolonged extension and the formation of a broader hyper-extended crust, largely due to the increased ductile deformation in the lower crust, as revealed in previous studies (Buck 1991; Huismans and Beaumont 2003;

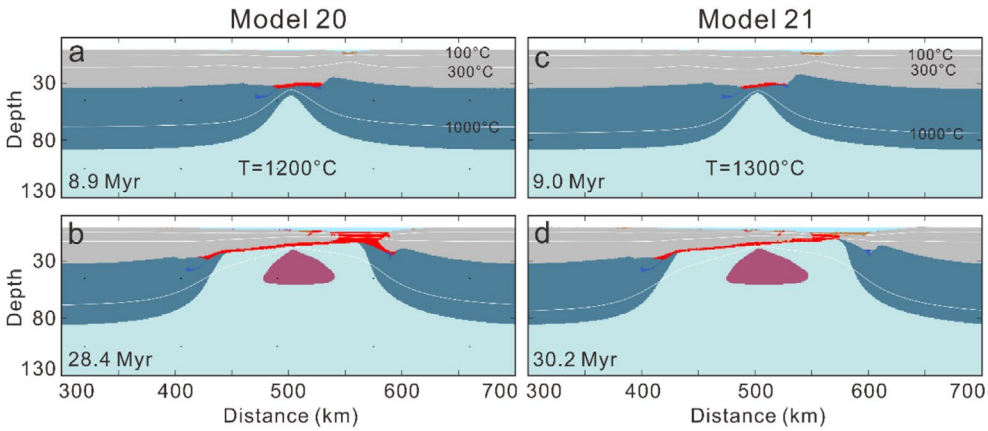

FIGURE 9 | Evolution of models featuring a felsic lower crust with different basal lithospheric mantle temperatures. (a) and (b) are evolution of model 20 with temperature of 1200 °C, (c) and (d) are evolution of model 21 with temperature of 1300°C.

Gouiza and Paton 2019). Numerical modelling indicates that a weaker felsic lower crust extends the rifting duration to approximately 30 Ma, which is significantly longer than that of a plagioclase-rich lower crust and aligns more closely with the rifting history of the SCS. The weaker rheology in the SCS lower crust is attributed to pre-rift processes, such as crustal deformation and magmatic additions during the Mesozoic (Brune et al. 2017). In addition, the subduction of the Izanagi plate is also thought to have triggered magma upwelling, which heated the lithosphere and lowered crustal viscosity (Li et al. 2018; Bai et al. 2020).

Prolonged extension, facilitated by reduced lithospheric strength, allows for extended heating periods, significantly elevating crustal temperatures. This results in a broader distribution of crustal melts at the end of numerical simulations. The melts are predominantly concentrated beneath hyper-extended domains, especially where the crust is less than 20 km thick. In the northern SCS margin, the thin-crust domains exhibit notably high surface heat flow, reaching up to approximately 120 mW/m^2. This observed heat flow anomaly is driven by two primary processes: (1) intense crustal thinning, which enhances mantle ascent and heat transfer (Huismans et al. 2001; Li et al. 2019); and (2) continuous upwelling of hot asthenosphere, maintaining elevated geothermal gradients during continental breakup (Lei 2013; Shi et al. 2017). In essence, the interplay between crustal thinning and mantle upwelling increases heat flow and promotes crustal melt generation, particularly in hyper-extended regions. Our models confirm these findings and further demonstrate that the initially weak SCS lithosphere, particularly the weaker lower crust, acts as a key factor in facilitating the interaction between crustal thinning, mantle dynamics, and melting generation during continental breakup.

5.2 | Numerical Results Summary

In contrast to previous models of magma-rich margins that employed a mantle plume beneath the continent (e.g., Koptev et al. 2021), we used a homogeneous model with extensional velocities on both sides to simulate the passive extension of the lithosphere at a magma-intermediate margin. Our findings demonstrate the feasibility of crustal melting at passive margins. The preferential removal of mantle lithosphere during rifting emerges as a crucial factor for crustal melting, as it enables the crust to receive sufficient heat from the upwelling asthenosphere to reach its solidus temperature. The condition aligns with the findings of Lu and Huismans (2022), who reported a similar prerequisite for melt generation in rifted magma-rich margins, where the rupture of the lithospheric mantle must precede that of the crust. In the SCS, recent work using OBS and reflection seismic profiles (Zhang et al. 2023) has shown that the mantle lithosphere was removed before the crust. Our model results agree with these findings and extend these conditions to encompass crustal melting in magma-intermediate margins.

Our modelling reveals a distinct deformation pattern, with the lithospheric mantle undergoing pure shear deformation while the crust experiences simple shear (Figure 10a). The onset of crustal melting coincides with the initial rupture point of the lithospheric mantle, and the melt zone subsequently propagates

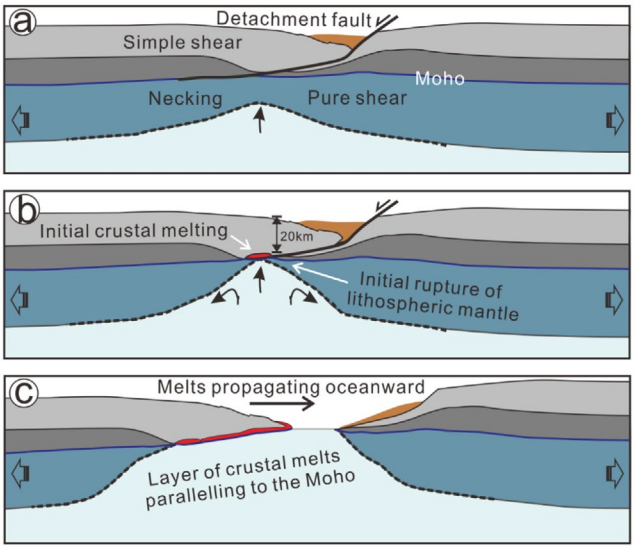

FIGURE 10 | Schematic illustration showing the evolution of crustal melts at a magma-intermediate margin during late stages of syn-rift. (a) The contrasting deformation patterns of the crust (simple shear) and lithospheric mantle (pure shear). (b) The initiation of crustal melts at the point of lithospheric mantle rupture, where the crustal thickness is less than 20 km. (c) The seaward propagation of crustal melts, ultimately forming layers parallel to the Moho.

oceanward. This implies a progressive younging of the melts towards the ocean, ultimately manifesting as layers parallel to the Moho (Figure 10c). The crustal melts predominantly occur beneath the thin-crust domain, specifically where the crust is less than 20 km thick. These observations align with phenomena documented along the SCS margin and are further corroborated by studies from other rifted margins. These studies highlight the presence of distinct, elongated magmatic intrusions within the COT zone, which exhibit a progressive increase in volume towards the ocean (Russell and Whitmarsh 2003; Pérez-Gussinyé et al. 2006; Ding et al. 2020; Zhang et al. 2021).

5.3 | Comparison With the Northern SCS Margin

The SCS margin, previously classified as magma-poor, has been re-evaluated due to recent seismic evidence indicating the presence of syn-rift magmatic materials. These findings suggest that the SCS represents an intermediate type between magma-poor and magma-rich margins (Sun et al. 2019; Ding et al. 2020; Pérez-Gussinyé et al. 2023), characterised by active volcanism during the rifting process, particularly in the late stages of syn-rift. Several ocean bottom seismometer (OBS) refraction seismic surveys, including OBS2001 (Wang et al. 2006), OBS2006-3 (Wei et al. 2011), OBST3 (Lester et al. 2014), T2933, OBS2012 (Wan et al. 2017), OBS2015-2 (Liu, Zhao, et al. 2018), OBS2016-2 (Wan et al. 2019), NS5 (Fan et al. 2019), have identified HVLs in the lower crust of the SCS, characterised by P-wave velocities ranging from approximately 6.9 to 7.5 km/s. These HVLs are interpreted as significant structural indicators of magmatic activity situated above the Moho. Recent studies have further divided the HVLs into two sections: one associated with the Mesozoic volcanic arc beneath the continental shelf, and the other linked to

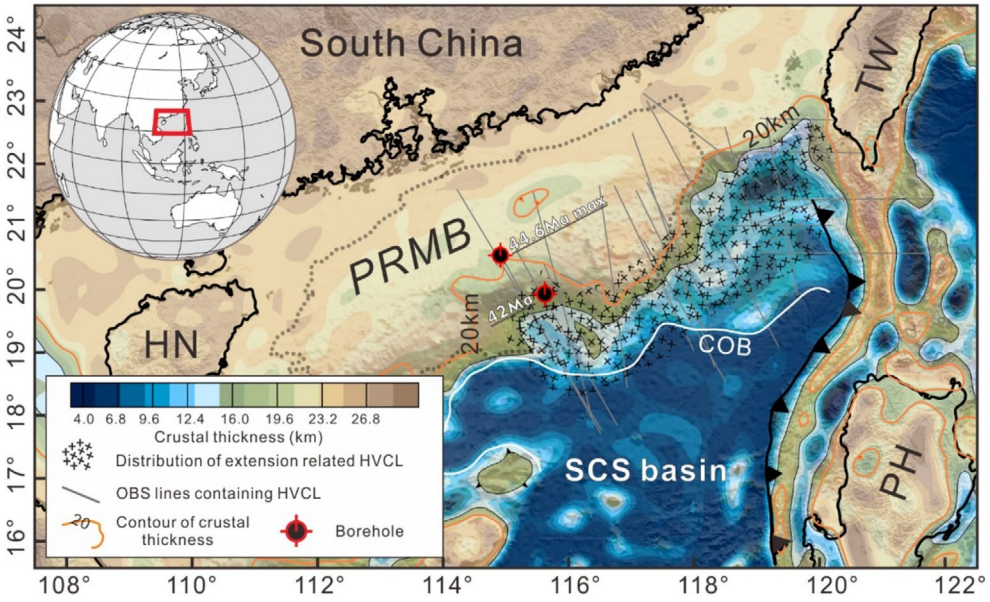

FIGURE 11 | Crustal thickness map of the northern SCS margin, illustrating the spatial distribution of Cenozoic rift-related HVLs and the ages of drilled igneous rocks. The potential distribution of rift-related HVLs is based on interpretations from various OBS surveys (Wang et al. 2006; Wei et al. 2011; Lester et al. 2014; Wan et al. 2017; Liu, Zhao, et al. 2018; Wan et al. 2019; Fan et al. 2019; etc.), while the crustal thickness contour is derived from Li et al. (2019). The ages of the drilling rocks are compiled from multiple sources (Qiu et al. 2013, 2016; Pang et al. 2022).

Cenozoic rift-related magmatism beneath the ultra-thinned crust in the COT (Wan et al. 2017; Li et al. 2018; Lei, Ren, et al. 2019; Cheng et al. 2021). Figure 11 illustrates the correlation between the distribution of potential rift-related magmatism and crustal thickness. The figure demonstrates that magmatic additions are primarily concentrated on the continental slope where the crustal thickness is less than 20 km. These observations align with the numerical modelling results, which indicate that the presence of melts is restricted to regions with thinned crust below 20 km in thickness.

As illustrated in Figure 11, the majority of rift-related HVLs are concentrated in the eastern region of the northern SCS margin. The pattern is consistent with previous research that has also identified a significant east–west contrast of HVLs in the extent of rift-related magmatism (Wan et al. 2017; Chen et al. 2022). The eastern margins, particularly the Pearl River Mouth Basin and Tainan Basin, exhibit a much higher abundance of HVLs compared to the western Qiongdongnan Basin. The Qiongdongnan Basin, on the other hand, shows a significantly lower occurrence of HVLs, which may be attributed to serpentinisation (Lei, Ren, et al. 2019). Our numerical results propose that the westward decrease in rift-related magmatism is primarily attributed to differential crustal stretching along the margin. The eastern region experienced greater extension, leading to the development of extensive thin-crust domains, which are conducive to melting generation. In contrast, the western region underwent less extension, resulting in the infrequent occurrence of crusts thinner than 20 km, a critical threshold for melt production in our models. The development of highly thinned crust in the SCS margin is likely influenced by a multitude of factors, including variations in crustal structure (e.g., Li et al. 2019), extension velocity (e.g., Pérez-Gussinyé et al. 2016), the style of breakup (plate-edge or plate-interior) (e.g., Wang et al. 2019; Li et al. 2020), water content in the for-arc or arc domain (e.g., Sun et al. 2021), and the inheritance of pre-existing structures (e.g., Huang et al. 2019).

The thickness of crustal melts predicted by our models was found to be less than the observed thickness of HVLs (7–10 km) in the seismic profiles. Considering that both asthenospheric and crustal melts contribute to rift-related magmatism in the SCS margin, it is plausible that the additional thickness in the HVLs is due to decompression melts from the rising asthenosphere. By subtracting the modelled crustal melt thickness from the observed HVL thickness, we estimate that asthenospheric magma constitutes approximately 70%–85% of the HVLs, while crustal melt accounts for the remaining 15%–30%.

The recent increase in industrial exploration has revealed igneous rocks intruded during the syn-rift to early post-rift period of the SCS margin. Two boreholes, PY24-1-1 and L-6, located in the thin-crust domain (characterised by a thickness of less than 20 km) and exhibiting typical igneous characteristics, were selected to determine the timing of melting. These boreholes contain igneous rocks emplaced during the syn-rift magmatism, dated at 42 Ma and 44.6 Ma, respectively (Li et al. 1999; Qiu et al. 2016; Pang et al. 2022). The age variation indicates a southward (oceanward) younging trend in magmatism within the northern SCS margin (Figure 10). Previous models attributed the late syn-rift to early post-rift magmatic activity in the northern SCS to either southeastward mantle flow induced by the Indo-Eurasian collision or the southward migration of the Hainan Plume (Xia et al. 2016; Zhang et al. 2018; Yu et al. 2018). However, while these mechanisms can explain the generation of decompression melts, they do not account for the presence of crustal melts, which have a distinct origin. Our numerical results support the interpretation that the younger–oceanward trend of magmatism is a consequence of the progressive

exposure of the crust to the hot asthenosphere as extension proceeded from north to south.

5.4 | Comparison With the Southern SCS Margin

Numerous geophysical surveys have been conducted to investigate the crustal structure of the SCS margin. However, the spatial coverage of these studies remains uneven, with significantly fewer surveys in the southern SCS compared to the northern region. Seismic refraction studies have revealed that HVLs at the COT are predominantly found in the northern SCS margin, whereas no HVLs have been observed in the southern margin (Nissen et al. 1995; Yan et al. 2006; Wang et al. 2006; Wei et al. 2011; Pichot et al. 2014; Chang et al. 2024). This suggests fundamental differences in the tectono-magmatic processes between the conjugate margins of the SCS.

The continental breakup in the SCS is asymmetric. In the northern SCS, the hyper-extended continental crust is significantly wider and is accompanied by extensive magmatism beneath it. In contrast, the southern SCS margin exhibits a more abrupt transition in crustal thickness from the continental to the oceanic domain, with oceanward-dipping

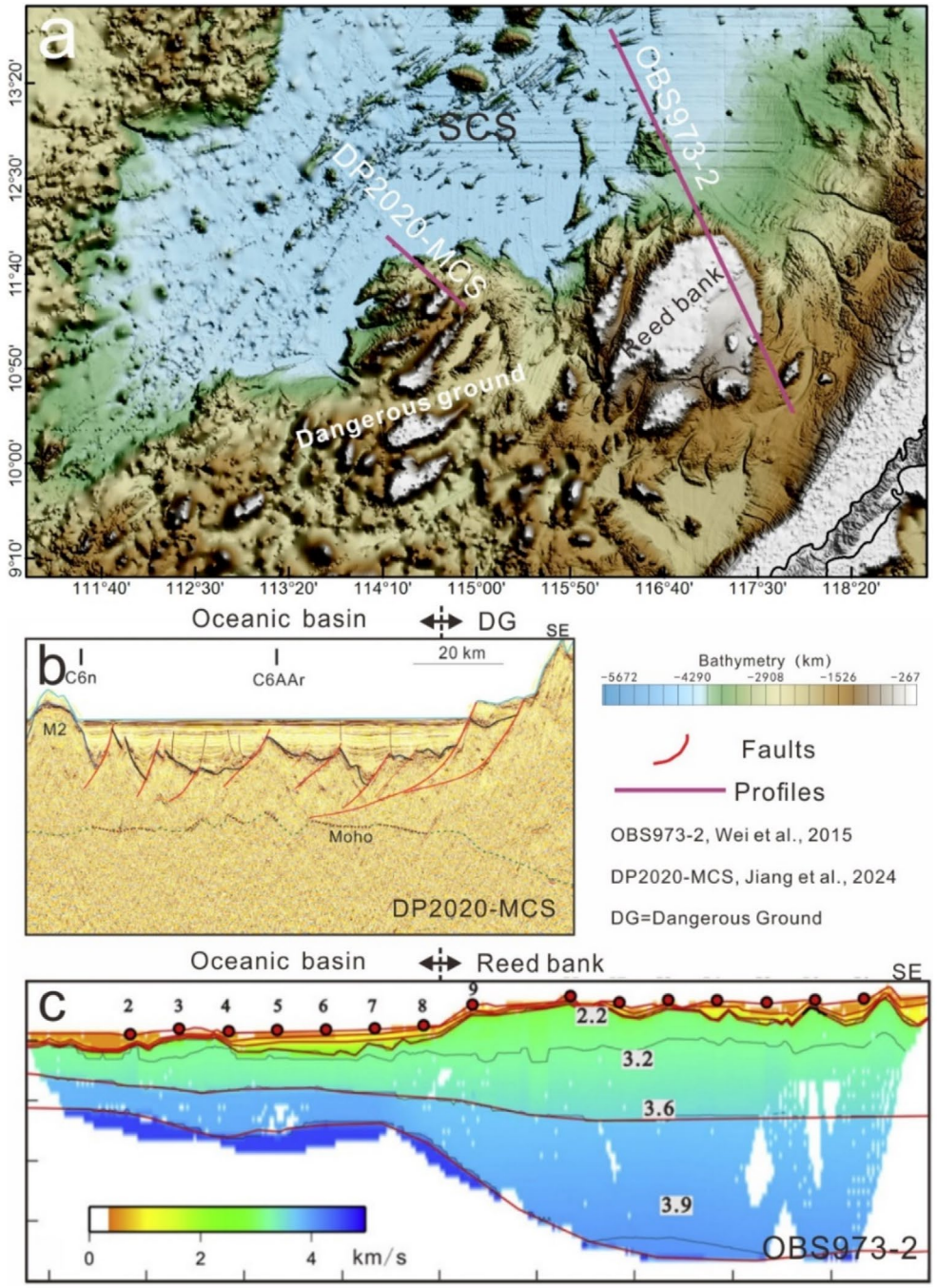

FIGURE 12 | Bathymetry of the southern SCS margin (a) with reflection seismic profile DP2020-MCS (b) and refraction seismic profile OBS973-2 (c), illustrating the lithospheric characteristics (Wei et al. 2015; Jiang et al. 2024).

syn-rift faults developing within the continental crust (Jiang et al. 2024) (Figure 12b). P-wave velocity models further illustrate the asymmetry, indicating that the southern SCS retains a relatively normal lithospheric structure. The Moho depth varies from approximately 20–22 km beneath the Reed Bank to around 9–11 km in the oceanic basin, with no evidence of HVLs, thin or absent sedimentary cover, and a characteristic continental crustal stratigraphy (Wei et al. 2015) (Figure 12c). These observations contrast sharply with those of the northern margin, where significant lower crustal magmatic intrusions have been identified.

Our numerical modelling results provide additional insights into the nature of the asymmetry, revealing that magmatic activity and crustal melts are primarily concentrated on the left-hand side of the rift (northern SCS). In contrast, the right-hand margin (southern SCS) is narrower and retains the lithospheric mantle, consistent with previous studies (e.g., Brune et al. 2014). The presence of this preserved lithospheric mantle in the southern SCS acts as a thermal barrier, inhibiting the transfer of heat into the crust. Consequently, the southern SCS margin experiences limited or negligible crustal melting. The thermal and mechanical asymmetry aligns well with geophysical observations, which show an absence of magmatic underplating and a sharper transition from continental to oceanic crust along the southern SCS margin. These findings suggest that the contrasting lithospheric configurations of the conjugate margins play a critical role in governing the magmatic evolution of the SCS.

5.5 | Model Limitations

Numerical models are strongly dependent on initial and boundary conditions, which influence the accuracy and applicability of the predictions. In our simulations, we conducted sensitivity analyses on key parameters, including extension velocity, thermal structure, lithospheric rheology, and crustal composition (e.g., felsic vs. plagioclase-rich lower crust), to evaluate their effects on the final crustal architecture and magmatic activity in rifted margins. As demonstrated in the results section, rapid extension rates and weaker lithospheric rheology, such as the presence of a felsic lower crust, tend to promote extensive crustal thinning and a broader zone of magmatic addition. However, several factors that could further impact magmatic budgets were not explicitly incorporated due to our model simplifications. For instance, our models did not account for pre-rift structural inheritance, which plays a crucial role in rift asymmetry. The presence of ancient sutures and inherited lithospheric heterogeneities can significantly influence strain localization and differential magmatic activity along conjugate margins (Gouiza and Naliboff 2021). Future models incorporating such structural complexities may provide a more accurate representation of natural rift evolution. Nevertheless, despite these simplifications, our results can offer a first-order approximation of crustal magmatic activity in a magma-intermediate margin under an idealised homogeneous setting.

To localise deformation, we introduced a weak zone in the initial model setup. Consequently, our simulations primarily represent the late-stage rift evolution leading to continental breakup rather than the entire rifting process. Although our models do not capture the full rifting history, the limitation does not affect the relevance of our findings regarding magmatic processes in the SCS margin. Seismic studies indicate that magmatic additions within the COT occur as rapid events during the final stages of continental extension (Larsen et al. 2018; Ding et al. 2020; Nirrengarten et al. 2020). Since our models focus on this crucial time frame, the results remain effective in capturing the key processes governing the magmatic additions. Another important consideration is our assumption of a constant extension rate. Previous studies have suggested that rift evolution may involve an initial slow phase followed by a sharp acceleration before continental breakup (Brune et al. 2016; Ulvrova et al. 2019). While our models adopt a constant velocity approach, we explore a broad range of extension rates, from slow to rapid, to assess their first-order effects. The approach is effective in capturing the sensitivity of magmatic processes to extension velocity. Furthermore, since our study primarily focuses on the late-stage syn-rift evolution of the SCS, the use of a constant velocity remains a reasonable approximation for understanding the associated crustal melting events.

Additionally, mantle dynamics remain a significant source of uncertainty in our models. Natural rifting environments likely involve complex interactions between small-scale convection, asthenospheric flow, and melt migration (Faccenna et al. 2014), which we approximate using a simplified, uniform asthenospheric flow pattern. While our models predict the spatial distribution and volume of magmatic additions under idealised conditions, future work integrating advanced thermomechanical coupling and dynamic mantle flow simulations could provide a more realistic representation of these processes.

Finally, while our 2-D models capture key aspects of crustal melting events during the late stage of rifting, the models fail to represent the full 3-D complexity of magmatic systems. Magmatic processes, including the distribution of HVL bodies, exhibit significant along-strike variations that cannot be fully addressed in a 2-D framework. To overcome this limitation, future research should employ 3-D numerical modelling, allowing for a more comprehensive assessment of spatial variations and facilitating direct comparisons with observed HVLs along the SCS margin. Addressing these uncertainties in future studies will enhance the robustness of numerical predictions and improve our ability to reconstruct the geodynamic evolution of passive margins.

6 | Conclusion

The numerical modelling presented in this study provides valuable insights into the processes governing crustal melting and the formation of HVLs in magma-intermediate margins, exemplified by the SCS margin. The models highlight the critical role of preferential lithospheric mantle removal in facilitating crustal melting by enabling sufficient heat transfer from the upwelling asthenosphere. The resulting melts accumulate beneath the thinned crust, forming layers parallel to the Moho, and exhibit a younger-oceanward age progression due to the progressive exposure of the crust to the hot asthenosphere during rifting. The extent and distribution of crustal melts are shown to be influenced by both extension velocity and crustal rheology.

Comparison of modelling results with seismic observations from the SCS margin supports the predictions of models, demonstrating the presence of crustal melts beneath thinned crust (< 20 km) and a similar age progression. The models also quantify the contribution of crustal melts to HVLs, suggesting crustal melts account for approximately 15%–30%, with the remainder attributed to asthenospheric magma.

Acknowledgements

We would like to express our sincere gratitude to Associate Editor Peter Burgess, Reviewer Prof. Chao Lei, Reviewer Prof. Mohamed Gouiza, and the anonymous reviewer for their constructive comments, which have greatly contributed to improving our manuscript. This research was supported by the Ministry of Science and Technology of China (2023YFF0803402), NSFC Major Research Plan on West-Pacific Earth System Multispheric Interactions (92158205), the Hainan Provincial Natural Science Foundation of China (422MS161); the Guangdong Natural Science Foundation (2022A1515011921, 2023A151500124); the Key Laboratory of Marine Mineral Resources, Ministry of Natural Resources, Guangzhou (KLMMR-2022-G04). Figures were made using perceptually uniform diverging colormaps (Crameri et al. 2020) and GMT (Wessel et al. 2013).

Conflicts of Interest

The authors declare no conflicts of interest.

Data Availability Statement

Data can be obtained from a repository: 10.6084/m9.figshare.22092851.

References

Aslanian, D., M. Moulin, J.-L. Olivet, et al. 2009. "Brazilian and African Passive Margins of the Central Segment of the South Atlantic Ocean: Kinematic Constraints." *Tectonophysics* 468, no. 1–4: 98–112.

Bai, Y., X. Wang, D. Dong, S. Brune, S. Wu, and Z. Wang. 2020. "Symmetry of the South China Sea Conjugate Margins in a Rifting, Drifting and Collision Context." *Marine and Petroleum Geology* 117: 104397.

Barckhausen, U., and H. A. Roeser. 2004. "Seafloor Spreading Anomalies in the South China Sea Revisited: Continent-Ocean Interactions Within East Asian Marginal Seas." 149: 121–125.

Bialas, R. W., and W. R. Buck. 2009. "How Sediment Promotes Narrow Rifting: Application to the Gulf of California." *Tectonics* 28, no. 4: TC4014.

Bronner, A., D. Sauter, G. Manatschal, G. Péron-Pinvidic, and M. Munschy. 2011. "Magmatic Breakup as an Explanation for Magnetic Anomalies at Magma-Poor Rifted Margins." *Nature Geoscience* 4, no. 8: 549–553.

Brune, S., and J. Autin. 2013. "The Rift to Break-Up Evolution of the Gulf of Aden: Insights From 3D Numerical Lithospheric-Scale Modelling." *Tectonophysics* 607: 65–79.

Brune, S., C. Heine, P. D. Clift, and M. Pérez-Gussinyé. 2017. "Rifted Margin Architecture and Crustal Rheology: Reviewing Iberia-Newfoundland, Central South Atlantic, and South China Sea." *Marine and Petroleum Geology* 79: 257–281.

Brune, S., C. Heine, M. Pérez-Gussinyé, and S. V. Sobolev. 2014. "Rift Migration Explains Continental Margin Asymmetry and Crustal Hyper-Extension." *Nature Communications* 5: 4014.

Brune, S., S. E. Williams, N. P. Butterworth, and R. D. Müller. 2016. "Abrupt Plate Accelerations Shape Rifted Continental Margins." *Nature* 536, no. 7615: 201–204.

Buck, W. R. 1991. "Modes of Continental Lithospheric Extension." *Journal of Geophysical Research: Solid Earth* 96: 20161–20178.

Burov, E., and S. A. P. L. Cloetingh. 1997. "Erosion and Rift Dynamics: New Thermomechanical Aspects of Post-Rift Evolution of Extensional Basins." *Earth and Planetary Science Letters* 150, no. 1-2: 7–26.

Chang, J. H., Z. L. Hong, A. Mirza, et al. 2024. "Spatial Distribution and Possible Origin of the High Velocity Lower Crust in the Northern Margin of the South China Sea." *Geoscience Letters* 11, no. 1: 51.

Chen, S.-S., J. Chen, Z. Guo, T. Wu, J. Liu, and R. Gao. 2022. "Magma Evolution of the South China Sea Basin From Continental-Margin Rifting to Oceanic Crustal Spreading: Constraints From In-Situ Trace Elements and Sr Isotope of Minerals." *Chemical Geology* 589: 120680.

Cheng, J., J. Zhang, M. Zhao, et al. 2021. "Spatial Distribution and Origin of the High-Velocity Lower Crust in the Northeastern South China Sea." *Tectonophysics* 819: 229086.

Coffin, M. F., and O. Eldholm. 1994. "Large Igneous Provinces: Crustal Structure, Dimensions, and External Consequences." *Reviews of Geophysics* 32, no. 1: 1–36.

Contreras, J., R. Zühlke, S. Bowman, and T. Bechstädt. 2010. "Seismic Stratigraphy and Subsidence Analysis of the Southern Brazilian Margin (Campos, Santos and Pelotas Basins)." *Marine and Petroleum Geology* 27, no. 9: 1952–1980.

Crameri, F., and B. J. Kaus. 2010. "Parameters That Control Lithospheric-Scale Thermal Localization on Terrestrial Planets." *Geophysical Research Letters* 37, no. 9: L09308.

Crameri, F., G. E. Shephard, and P. J. Heron. 2020. "The Misuse of Colour in Science Communication." *Nature Communications* 11, no. 1: 1–10.

Crameri, F., P. Tackley, I. Meilick, T. Gerya, and B. Kaus. 2012. "A Free Plate Surface and Weak Oceanic Crust Produce Single-Sided Subduction on Earth." *Geophysical Research Letters* 39, no. 3: L03306.

Deng, P., L. Mei, J. Liu, et al. 2019. "Episodic Normal Faulting and Magmatism During the Syn-Spreading Stage of the Baiyun Sag in Pearl River Mouth Basin: Response to the Multi-Phase Seafloor Spreading of the South China Sea." *Marine Geophysical Researches* 40, no. 1: 33–50.

Deng, H., J. Ren, X. Pang, et al. 2020. "South China Sea Documents the Transition From Wide Continental Rift to Continental Break Up." *Nature Communications* 11, no. 1: 1–9.

Ding, W., Z. Sun, G. Mohn, et al. 2020. "Lateral Evolution of the Rift-To-Drift Transition in the South China Sea: Evidence From Multi-Channel Seismic Data and IODP Expeditions 367&368 Drilling Results." *Earth and Planetary Science Letters* 531: 115932.

Dong, D., S. Wu, J. Li, and T. Lüdmann. 2014. "Tectonic Contrast Between the Conjugate Margins of the South China Sea and the Implication for the Differential Extensional Model." *Science China Earth Sciences* 57, no. 6: 1415–1426.

Duclaux, G., R. S. Huismans, and D. A. May. 2020. "Rotation, Narrowing, and Preferential Reactivation of Brittle Structures During Oblique Rifting." *Earth and Planetary Science Letters* 531: 115952.

Espurt, N., J. P. Callot, F. Roure, J. M. Totterdell, H. I. Struckmeyer, and R. Vially. 2012. "Transition From Symmetry to Asymmetry During Continental Rifting: An Example From the Bight Basin–Terre Adélie (Australian and Antarctic Conjugate Margins)." *Terra Nova* 24, no. 3: 167–180.

Faccenna, C., T. W. Becker, L. Auer, et al. 2014. "Mantle Dynamics in the Mediterranean." *Reviews of Geophysics* 52: 283–332.

Fan, C., S. Xia, J. Cao, et al. 2019. "Lateral Crustal Variation and Post-Rift Magmatism in the Northeastern South China Sea Determined by Wide-Angle Seismic Data." *Marine Geology* 410: 70–87.

Fang, P., W. Ding, Y. Zhao, X. Lin, and Z. Zhao. 2022. "Detachment-Controlled Subsidence Pattern at Hyper-Extended Passive Margin:

Insights From Backstripping Modelling of the Baiyun Rift, Northern South China Sea." *Gondwana Research* 120: 70–84.

Franke, D. 2013. "Rifting, Lithosphere Breakup and Volcanism: Comparison of Magma-Poor and Volcanic Rifted Margins." *Marine and Petroleum Geology* 43: 63–87.

Gao, J., X. Peng, S. Wu, et al. 2019. "Different Expressions of the Crustal Structure Across the Dongsha Rise Along the Northeastern Margin of the South China Sea." *Journal of Asian Earth Sciences* 171: 187–200.

Geoffroy, L. 2005. "Volcanic Passive Margins." *Comptes Rendus Geoscience* 337, no. 16: 1395–1408. https://doi.org/10.1016/j.crte.2005.10.006.

Geoffroy, L., F. Chauvet, and J.-C. Ringenbach. 2022. "Middle-Lower Continental Crust Exhumed at the Distal Edges of Volcanic Passive Margins." *Communications Earth & Environment* 3, no. 1: 1–9.

Gerya, T. 2010. *Introduction to Numerical Geodynamic Modelling*. Cambridge University Press.

Gerya, T. V., and D. A. Yuen. 2007. "Robust Characteristics Method for Modelling Multiphase Visco-Elasto-Plastic Thermo-Mechanical Problems." *Physics of the Earth and Planetary Interiors* 163, no. 1–4: 83–105.

Gouiza, M., and J. Naliboff. 2021. "Rheological Inheritance Controls the Formation of Segmented Rifted Margins in Cratonic Lithosphere." *Nature Communications* 12, no. 1: 4653.

Gouiza, M., and D. A. Paton. 2019. "The Role of Inherited Lithospheric Heterogeneities in Defining the Crustal Architecture of Rifted Margins and the Magmatic Budget During Continental Breakup." *Geochemistry, Geophysics, Geosystems* 20: 1836–1853.

Hayes, D. E., and S. S. Nissen. 2005. "The South China Sea Margins: Implications for Rifting Contrasts." *Earth and Planetary Science Letters* 237, no. 3-4: 601–616.

Hayes, D. E., S. S. Nissen, P. Buhl, et al. 1995. "Throughgoing Crustal Faults Along the Northern Margin of the South China Sea and Their Role in Crustal Extension." *Journal of Geophysical Research: Solid Earth* 100: 22435–22446.

He, L., L. Xiong, and J. Wang. 2002. "Heat Flow and Thermal Modeling of the Yinggehai Basin, South China Sea." *Tectonophysics* 351, no. 3: 245–253.

Heine, C., J. Zoethout, and R. D. Müller. 2013. "Kinematics of the South Atlantic Rift." *Solid Earth* 4: 215–253.

Huang, H., X. Qiu, T. Pichot, and M. Zhao. 2019. "Seismic Structure of the Northwestern Margin of the South China Sea: Implication for Asymmetric Continental Extension." *Geophysical Journal International* 218, no. 2: 1246–1261.

Huismans, R. S., and C. Beaumont. 2003. "Symmetric and Asymmetric Lithospheric Extension: Relative Effects of Frictional-Plastic and Viscous Strain Softening." *Journal of Geophysical Research* 108, no. B10: 22.

Huismans, R. S., Y. Y. Podladchikov, and S. Cloetingh. 2001. "Transition From Passive to Active Rifting: Relative Importance of Asthenospheric Doming and Passive Extension of the Lithosphere." *Journal of Geophysical Research: Solid Earth* 106: 11271–11291.

Jiang, W., L. Wang, F. Li, B. Liu, and J. Zhao. 2024. "The Crustal Structure of the Southwestern South China Sea From Seismic Reflection and Refraction Data: Implications to Continental Breakup, Slow-Spreading Ridges, and Subsequent Mantle Activity." *Interpretation* 12: SA1–SA15.

Koptev, A., S. Cloetingh, I. J. Kovács, T. Gerya, and T. A. Ehlers. 2021. "Controls by Rheological Structure of the Lithosphere on the Temporal Evolution of Continental Magmatism: Inferences From the Pannonian Basin System." *Earth and Planetary Science Letters* 565: 116925.

Larsen, H. C., G. Mohn, M. Nirrengarten, et al. 2018. "Rapid Transition From Continental Breakup to Igneous Oceanic Crust in the South China Sea." *Nature Geoscience* 11, no. 10: 782–789.

Le Pourhiet, L., N. Chamot-Rooke, M. Delescluse, D. A. May, L. Watremez, and M. Pubellier. 2018. "Continental Break-Up of the South China Sea Stalled by Far-Field Compression." *Nature Geoscience* 11, no. 8: 605–609.

Lei, X. 2013. *Studies on the Heat Flow and Thermo-Mechanism of the Lithosphere in the Northern South China Sea Margin*, 1–5. Nanjing University.

Lei, C., T. M. Alves, J. Ren, X. Pang, L. Yang, and J. Liu. 2019. "Depositional Architecture and Structural Evolution of a Region Immediately Inboard of the Locus of Continental Breakup (Liwan Sub-Basin, South China Sea)." *GSA Bulletin* 131, no. 7–8: 1059–1074.

Lei, C., T. M. Alves, J. Ren, and C. Tong. 2020. "Rift Structure and Sediment Infill of Hyperextended Continental Crust: Insights From 3D Seismic and Well Data (Xisha Trough, South China Sea)." *Journal of Geophysical Research: Solid Earth* 125, no. 5: e2019JB018610. https://doi.org/10.1029/2019JB018610.

Lei, C., J. Ren, and X. Pang. 2019. "Rift Structures and Its Related Unconformities on and Adjacent the Dongsha Rise: Insights Into the Nature of the High-Velocity Layer in the Northern South China Sea." *Marine Geophysical Research* 40: 99–110.

Lester, R., H. J. Van Avendonk, K. McIntosh, et al. 2014. "Rifting and Magmatism in the Northeastern South China Sea from Wide-Angle Tomography and Seismic Reflection Imaging." *Journal of Geophysical Research: Solid Earth* 119, no. 3: 2305–2323.

Li, J. 2011. "Dynamics of the Continental Margins in South China Sea: Scientific Experiments and Research Progresses." *Chinese Journal of Geophysics* 54, no. 6: 883–893.

Li, P., and H. Liang. 1994. "Cenozoic Magmatism in the Pearl River Mouth Basin and Its Relationship to the Basin Evolution and Petroleum Accumulation." *Guangdong Geology* 9, no. 2: 23–34. (in Chinese with English abstract).

Li, P. L., H. X. Liang, Y. D. Dai, and H. M. Lin. 1999. "Origin and Tectonic Setting of the Yanshanian Igneous Rocks in the Pearl River Mouth Basin." *Guangdong Geology* 14, no. 1: 1–8.

Li, F., Z. Sun, X. Pang, et al. 2019. "Low-Viscosity Crustal Layer Controls the Crustal Architecture and Thermal Distribution at Hyperextended Margins: Modeling Insight and Application to the Northern South China Sea Margin." *Geochemistry, Geophysics, Geosystems* 20, no. 7: 3248–3267.

Li, F., Z. Sun, and H. Yang. 2018. "Possible Spatial Distribution of the Mesozoic Volcanic Arc in the Present-Day South China Sea Continental Margin and Its Tectonic Implications." *Journal of Geophysical Research: Solid Earth* 123, no. 8: 6215–6235.

Li, F., Z. Sun, H. Yang, et al. 2020. "Continental Interior and Edge Breakup at Convergent Margins Induced by Subduction Direction Reversal: A Numerical Modeling Study Applied to the South China Sea Margin." *Tectonics* 39, no. 11: e2020TC006409. https://doi.org/10.1029/2020TC006409.

Li, C. F., X. Xu, J. Lin, et al. 2014. "Ages and Magnetic Structures of the South China Sea Constrained by Deep Tow Magnetic Surveys and IODP Expedition 349." *Geochemistry, Geophysics, Geosystems* 15, no. 12: 4958–4983.

Liao, J., and T. Gerya. 2015. "From Continental Rifting to Seafloor Spreading: Insight From 3D Thermo-Mechanical Modeling." *Gondwana Research* 28: 1329–1343.

Liu, L., L. J. Liu, J. P. Morgan, Y.-G. Xu, and L. Chen. 2023. "New Constraints on Cenozoic Subduction Between India and Tibet." *Nature Communications* 14, no. 1: 1963.

Liu, L., J. P. Morgan, Y. G. Xu, and M. Menzies. 2018. "Craton Destruction Part II: Evolution of Cratonic Lithosphere After a Rapid Keel Delamination Event." *Journal of Geophysical Research: Solid Earth* 123, no. 11: 10069–10090.

Liu, Z., M. Pérez-Gussinyé, L. Rüpke, I. A. Muldashev, T. A. Minshull, and G. Bayrakci. 2022. "Lateral Coexistence of Ductile and Brittle Deformation Shapes Magma-Poor Distal Margins: An Example From the West Iberia-Newfoundland Margins." *Earth and Planetary Science Letters* 578: 117288.

Liu, S., M. Zhao, J.-C. Sibuet, et al. 2018. "Geophysical Constraints on the Lithospheric Structure in the Northeastern South China Sea and Its Implications for the South China Sea Geodynamics." *Tectonophysics* 742: 101–119.

Lu, G., and R. S. Huismans. 2022. "Magmatism at Passive Margins: Effects of Depth-Dependent Wide Rifting and Lithospheric Counterflow." *Journal of Geophysical Research: Solid Earth* 127, no. 3: e2021JB023046.

Lundin, E. R., A. G. Doré, and T. F. Redfield. 2018. "Magmatism and Extension Rates at Rifted Margins." *Petroleum Geoscience* 24, no. 4: 379–392.

Ma, Y., S. Li, J. Lin, Q. Liang, Y. Shi, and L. Kong. 2016. "Magma Emplacement: An Important Trigger Leading to Slope Failures in Deep-Water Areas of Northern Continental Margin of South China Sea." *Geological Journal* 51: 96–107.

Ma, Q., J.-P. Zheng, Y.-G. Xu, W. L. Griffin, and R.-S. Zhang. 2015. "Are Continental "Adakites" Derived From Thickened or Foundered Lower Crust?" *Earth and Planetary Science Letters* 419: 125–133.

Menzies, M. A., S. L. Klemperer, C. J. Ebinger, and J. Baker. 2002. "Characteristics of Volcanic Rifted Margins." *Special Papers - Geological Society of America* 362: 1–14.

Moore, C., T. Wright, and A. Hooper. 2021. "Rift Focusing and Magmatism During Late-Stage Rifting in Afar." *Journal of Geophysical Research: Solid Earth* 126: e2020JB021542.

Naliboff, J., and S. J. Buiter. 2015. "Rift Reactivation and Migration During Multiphase Extension." *Earth and Planetary Science Letters* 421: 58–67.

Nirrengarten, M., G. Mohn, N. Kusznir, et al. 2020. "Extension Modes and Breakup Processes of the Southeast China-Northwest Palawan Conjugate Rifted Margins." *Marine and Petroleum Geology* 113: 104123.

Nissen, S. S., D. E. Hayes, P. Buhl, et al. 1995. "Deep Penetration Seismic Soundings Across the Northern Margin of the South China Sea." *Journal of Geophysical Research: Solid Earth* 100, no. B11: 22407–22433.

Pang, X., J. Zheng, J. Ren, et al. 2022. "Structural Evolution and Magmatism of Fault Depression in Baiyun Sag, Northern Margin of South China Sea." *Earth Science* 47, no. 7: 2303–2316. [in Chinese with English abstract].

Pérez-Gussinyé, M. 2013. "A Tectonic Model for Hyperextension at Magma-Poor Rifted Margins: An Example From the West Iberia–Newfoundland Conjugate Margins." *Geological Society, London, Special Publications* 369, no. 1: 403–427.

Pérez-Gussinyé, M., J. S. Collier, J. J. Armitage, J. R. Hopper, Z. Sun, and C. Ranero. 2023. "Towards a Process-Based Understanding of Rifted Continental Margins." *Nature Reviews Earth and Environment* 4, no. 3: 1–19.

Pérez-Gussinyé, M., J. P. Morgan, T. J. Reston, and C. R. Ranero. 2006. "The Rift to Drift Transition at Non-Volcanic Margins: Insights From Numerical Modelling." *Earth and Planetary Science Letters* 244, no. 1–2: 458–473.

Péron-Pinvidic, G., and G. Manatschal. 2009. "The Final Rifting Evolution at Deep Magma-Poor Passive Margins From Iberia-Newfoundland: A New Point of View." *International Journal of Earth Sciences* 98, no. 7: 1581–1597.

Pichot, T., M. Delescluse, N. Chamot-Rooke, et al. 2014. "Deep Crustal Structure of the Conjugate Margins of the SW South China Sea From Wide-Angle Refraction Seismic Data." *Marine and Petroleum Geology* 58: 627–643.

Planke, S., P. A. Symonds, E. Alvestad, and J. Skogseid. 2000. "Seismic Volcanostratigraphy of Large-Volume Basaltic Extrusive Complexes on Rifted Margins." *Journal of Geophysical Research: Solid Earth* 105, no. B8: 19335–19351.

Poli, S., and M. W. Schmidt. 2002. "Petrology of Subducted Slabs." *Annual Review of Earth and Planetary Sciences* 30, no. 1: 207–235.

Qiu, Y., L. Wang, and W. Huang. 2016. *Mesozoic Cenozoic Sedimentary Basins in China Sea Area*, 1–233. Geological Publishing House.

Qiu, H., J. Wei, and Y. Xu. 2013. "Preliminary Results of 40Ar/39Ar Dating of Daimao Hill Volcanic Rocks in the South China Sea." Proceedings of 2013 Annual Symposium on "The Evolution of Deep Sea Processes in the South China Sea", Vol. 16, Shanghai.

Ren, J. Y., X. Pang, Y. Peng, L. Chao, and L. Pan. 2018. "Characteristics and Formation Mechanism of Deepwater and Ultra-Deepwater Basins in the Northern Continental Margin of the South China Sea." *Chinese Journal of Geophysics* 61: 4901–4920.

Reston, T. 2009. "The Structure, Evolution and Symmetry of the Magma-Poor Rifted Margins of the North and Central Atlantic: A Synthesis." *Tectonophysics* 468, no. 1–4: 6–27.

Ros, E., M. Pérez-Gussinyé, M. Araújo, M. T. Romeiro, M. Andrés-Martínez, and J. P. Morgan. 2017. "Lower Crustal Strength Controls on Melting and Serpentinization at Magma-Poor Margins: Potential Implications for the South Atlantic." *Geochemistry, Geophysics, Geosystems* 18, no. 12: 4538–4557.

Russell, S., and R. Whitmarsh. 2003. "Magmatism at the West Iberia Non-Volcanic Rifted Continental Margin: Evidence From Analyses of Magnetic Anomalies." *Geophysical Journal International* 154, no. 3: 706–730.

Savva, D., M. Pubellier, D. Franke, et al. 2014. "Different Expressions of Rifting on the South China Sea Margins." *Marine and Petroleum Geology* 58: 579–598.

Schmidt, M. W., and S. Poli. 1998. "Experimentally Based Water Budgets for Dehydrating Slabs and Consequences for Arc Magma Generation." *Earth and Planetary Science Letters* 163, no. 1–4: 361–379.

Shi, X. B., C. H. Yu, M. Chen, X. Q. Yang, and J. F. Zhao. 2017. "Analyses of Variation Features and Influential Factors of Heat Flow in the Northern Margin of the South China Sea." *Earth Science Frontiers* 24, no. 3: 56–64. [in Chinese with English abstract].

Song, X., C.-F. Li, Y. Yao, and H. Shi. 2017. "Magmatism in the Evolution of the South China Sea: Geophysical Characterization." *Marine Geology* 394: 4–15.

Streckeisen, A. 1979. "Classification and Nomenclature of Volcanic Rocks, Lamprophyres, Carbonatites, and Melilitic Rocks: Recommendations and Suggestions of the IUGS Subcommission on the Systematics of Igneous Rocks." *Geology* 7, no. 7: 331–335. https://doi.org/10.1130/0091-7613(1979)7<>2.0.CO;2.

Sun, Q., T. M. Alves, M. Zhao, J.-C. Sibuet, G. Calvès, and X. Xie. 2020. "Post-Rift Magmatism on the Northern South China Sea Margin." *GSA Bulletin* 132, no. 11–12: 2382–2396.

Sun, Z., F. Li, J. Lin, L. Sun, X. Pang, and J. Zheng. 2021. "The Rifting-Breakup Process of the Passive Continental Margin and Its Relationship With Magmatism: The Attribution of the South China Sea." *Earth Science* 46, no. 3: 770–789.

Sun, Z., J. Lin, N. Qiu, et al. 2019. "The Role of Magmatism in the Thinning and Breakup of the South China Sea Continental Margin: Special Topic: The South China Sea Ocean Drilling." *National Science Review* 6, no. 5: 871–876.

Taylor, B., and D. E. Hayes. 1983. "Origin and History of the South China Sea basin." *Geophysical Monograph Series* 27: 23–56.

Tetreault, J. L., and S. J. H. Buiter. 2018. "The Influence of Extension Rate and Crustal Rheology on the Evolution of Passive Margins From Rifting to Break-Up." *Tectonophysics* 746: 155–172.

Tugend, J., M. Gillard, G. Manatschal, et al. 2020. "Reappraisal of the Magma-Rich Versus Magma-Poor Rifted Margin Archetypes." *Geological Society, London, Special Publications* 476, no. 1: 23–47.

Ulvrova, M. M., S. Brune, and S. Williams. 2019. "Breakup Without Borders: How Continents Speed Up and Slow Down During Rifting." *Geophysical Research Letters* 46, no. 3: 1338–1347.

Viltres, R., S. Jónsson, J. Ruch, et al. 2020. "Kinematics and Deformation of the Southern Red Sea Region From GPS Observations." *Geophysical Journal International* 221: 2143–2154.

Wan, X., C. F. Li, M. Zhao, et al. 2019. "Seismic Velocity Structure of the Magnetic Quiet Zone and Continent-Ocean Boundary in the Northeastern South China Sea." *Journal of Geophysical Research: Solid Earth* 124, no. 11: 11866–11899.

Wan, K., S. Xia, J. Cao, J. Sun, and H. Xu. 2017. "Deep Seismic Structure of the Northeastern South China Sea: Origin of a High-Velocity Layer in the Lower Crust." *Journal of Geophysical Research: Solid Earth* 122, no. 4: 2831–2858.

Wang, T. K., M.-K. Chen, C.-S. Lee, and K. Xia. 2006. "Seismic Imaging of the Transitional Crust Across the Northeastern Margin of the South China Sea." *Tectonophysics* 412, no. 3–4: 237–254.

Wang, P., C. Y. Huang, J. Lin, Z. Jian, Z. Sun, and M. Zhao. 2019. "The South China Sea Is Not a Mini-Atlantic: Plate-Edge Rifting vs Intraplate Rifting." *National Science Review* 6, no. 5: 902–913.

Wang, H., Q. Zhao, S. Wu, D. Wang, and B. Wang. 2018. "Post-Rifting Magmatism and the Drowned Reefs in the Xisha Archipelago Domain." *Journal of Ocean University of China* 17, no. 1: 195–208.

Wei, X., A. Ruan, M. Zhao, et al. 2011. "A Wide-Angle Obs Profile Across the Dongsha Uplift and Chaoshan Depression in the Mid-Northern South China Sea." *Chinese Journal of Geophysics* 54, no. 6: 1149–1160.

Wei, X., A. Ruan, M. Zhao, X. Qiu, Z. Wu, and X. Niu. 2015. "Shear Wave Velocity Structure of Reed Bank, Southern Continental Margin of the South China Sea." *Tectonophysics* 644: 151–160.

Wessel, P., W. H. Smith, R. Scharroo, J. Luis, and F. Wobbe. 2013. "Generic Mapping Tools: Improved Version Released." *Eos, Transactions American Geophysical Union* 94, no. 45: 409–410.

White, R., and D. McKenzie. 1989. "Magmatism at Rift Zones: The Generation of Volcanic Continental Margins and Flood Basalts." *Journal of Geophysical Research: Solid Earth* 94, no. B6: 7685–7729.

Whitmarsh, R., G. Manatschal, and T. Minshull. 2001. "Evolution of Magma-Poor Continental Margins From Rifting to Seafloor Spreading." *Nature* 413, no. 6852: 150–154.

Xia, S., D. Zhao, J. Sun, and H. Huang. 2016. "Teleseismic Imaging of the Mantle Beneath Southernmost China: New Insights Into the Hainan Plume." *Gondwana Research* 36: 46–56.

Xiaoxi, Z., Z. Zhongxian, Z. Haiteng, et al. 2023. "Characteristics of Syn-Spread Magmatism and Its Implication for Tectonic Evolution in Baiyun-Liwan Deep-Water Area of Pearl River Mouth Basin." *Earth Science* 48, no. 10: 3781–3798. (in Chinses with English abstract).

Yan, P., H. Deng, H. Liu, Z. Zhang, and Y. Jiang. 2006. "The Temporal and Spatial Distribution of Volcanism in the South China Sea Region." *Journal of Asian Earth Sciences* 27, no. 5: 647–659.

Ye, Q., L. Mei, D. Jiang, et al. 2022. "3-D Structure and Development of a Metamorphic Core Complex in the Northern South China Sea Rifted Margin." *Journal of Geophysical Research: Solid Earth* 127, no. 2: e2021JB022595. https://doi.org/10.1029/2021JB022595.

Yu, M., Y. Yan, C. Y. Huang, et al. 2018. "Opening of the South China Sea and Upwelling of the Hainan Plume." *Geophysical Research Letters* 45, no. 6: 2600–2609.

Zeng, Z., H. Zhu, X. Yang, G. Zhang, and H. Zeng. 2019. "Three-Dimensional Imaging of Miocene Volcanic Effusive and Conduit Facies: Implications for the Magmatism and Seafloor Spreading of the South China Sea." *Marine and Petroleum Geology* 109: 193–207.

Zhang, G.-L., Q. Luo, J. Zhao, M. G. Jackson, L.-S. Guo, and L.-F. Zhong. 2018. "Geochemical Nature of Sub-Ridge Mantle and Opening Dynamics of the South China Sea." *Earth and Planetary Science Letters* 489: 145–155.

Zhang, C., Z. Sun, G. Manatschal, et al. 2021. "Syn-Rift Magmatic Characteristics and Evolution at a Sediment-Rich Margin: Insights From High-Resolution Seismic Data From the South China Sea." *Gondwana Research* 91: 81–96.

Zhang, Q., S. Wu, and D. Dong. 2016. "Cenozoic Magmatism in the Northern Continental Margin of the South China Sea: Evidence From Seismic Profiles." *Marine Geophysical Researches* 37, no. 2: 71–94.

Zhang, J., M. Zhao, Z. Sun, et al. 2023. "Large Volume of Magma Involved in South China Sea Rifting: Implication for Mantle Breakup Earlier Than Crust." *Tectonophysics* 853: 229801.

Zhao, M., E. He, J. C. Sibuet, et al. 2018. "Postseafloor Spreading Volcanism in the Central East South China Sea and Its Formation Through an Extremely Thin Oceanic Crust." *Geochemistry, Geophysics, Geosystems* 19, no. 3: 621–641.

Zhao, Y., J. Ren, X. Pang, L. Yang, and J. Zheng. 2018. "Structural Style, Formation of Low Angle Normal Fault and Its Controls on the Evolution of Baiyun Rift, Northern Margin of the South China Sea." *Marine and Petroleum Geology* 89: 687–700.

Zhao, Z., Z. Sun, N. Qiu, et al. 2022. "The Paleo-Lithospheric Structure and Rifting-Magmatic Processes of the Northern South China Sea Passive Margin." *Gondwana Research* 120: 162–174.

Zhao, F., S. Wu, Q. Sun, M. Huuse, W. Li, and Z. Wang. 2014. "Submarine Volcanic Mounds in the Pearl River Mouth Basin, Northern South China Sea." *Marine Geology* 355: 162–172.

Zhou, D., and B. Yao. 2009. "Tectonics and Sedimentary Basins of the South China Sea: Challenges and Progresses." *Journal of Earth Science* 20, no. 1: 1–12.

Supporting Information

Additional supporting information can be found online in the Supporting Information section.